

Published in

Marine and Petroleum Geology
Available online 14 October 2016

Forward modelling of carbonate platforms: sedimentological and diagenetic constraints from an application to a flat-topped greenhouse platform (Triassic, Southern Alps, Italy)

F. Berra¹, A. Lanfranchi^{1*}, P.L. Smart², F.F. Whitaker³, P. Ronchi⁴

1: Università degli Studi di Milano, Dip. Scienze della Terra "A. Desio", Milano, Italy (fabrizio.berra@unimi.it)

2: School of Geographical Sciences, University of Bristol, UK

3: School of Earth Sciences, University of Bristol, UK

4: ENI s.p.a., San Donato Milanese, Italy

*: present Address: Oolithica, Cheltenham, UK

Highlights

- We propose a quantitative analysis of a carbonate platform using 3d numerical models.
- Parameter definition is critical to produce realistic 3d numerical models.
- Modelling parameters were defined by architectural and sedimentological studies.
- The obtained model has been tested by comparison with outcrop and laboratory data.
- 3d numerical models may help to parameterise petrophysical properties of geobodies.

Key words: carbonate platform, forward modelling, Triassic, facies analysis, diagenesis

Abstract

Quantitative analysis of depositional systems using numerical models can provide insights into the interaction of sedimentological and diagenetic processes, difficult to interpret from observation of the geological products alone. Numerical models can highlight the interactions between controlling parameters, and generate best estimate simulations of case studies from the geological record. Different data sources (e.g., outcrop data, uniformitarian constraints, paleogeography) need to be considered in the process of defining the parameters required to produce models that honour individual case studies. We present a best-estimate forward model of a high-relief Triassic carbonate platform (Southern Alps, Italy) generated using CARB3D+, a 3D process-based forward modelling package able to simulate sedimentary facies, geometries and early diagenesis of isolated carbonate platforms. The parameters used for the presented forward model have been deduced by the study of architectural, sedimentological and diagenetic features of the platform, and by data from modern and ancient analogues. Sensitivity analysis is used to tune values of the parameters within ranges defined from field, laboratory and uniformitarian constraints. Critical evaluation of the model allowed 1) verification of the validity of the used parameters; 2) evaluation of the interaction between controlling parameters; 3) development of a numerical model that can be used for quantitative elaborations. Furthermore, the process of generating the numerical model required a detailed interpretation of field and laboratory data, crucial to define the required input parameters. Modelling the studied carbonate platform also enabled evaluation of the effects of the interaction between productivity, environmental energy and creation of accommodation space, promoting the understanding of their role on the architecture of carbonate systems. Forward modelling also allows the integration of data from conventional data sets with data from present-day observations and seismic geometries, promoting a transition from a qualitative to a semi-quantitative/quantitative sedimentological approach. Forward models can further be used to parameterise petrophysical properties of complex geobodies, with potential application for the management of georesources.

1. Introduction

The growth mode of carbonate platforms is strongly controlled by biological, climatic and environmental factors (e.g. Pomar & Hallock, 2008), as well as antecedent topography, tectonics (e.g. Bosence, 2005) and eustacy. The interplay of these factors is responsible for the platform geometry and the nature and distribution of depositional and diagenetic facies. Because of the considerable spatial and temporal variations in factors controlling platform evolution and the complex interactions between them, a wide range of depositional architectures is observed in the geological record. This precludes definition of a common behaviour for platforms at different times in the geological past and in different environments (Markello et al., 2008).

Information on the factors controlling the depositional architecture and facies distribution of carbonate systems derives from studies of both modern and ancient platforms. Studies of modern systems can elucidate the role played by environmental factors, such as current strength and direction, water temperature and nutrient levels on platform development (e.g. Hallock, 2001). Similarly, the study of fluid chemistry and flow in different hydrologically-controlled diagenetic zones (hydrozones; James & Choquette, 1988) provides information about the distribution, rate and drivers for early diagenesis (e.g. Whitaker & Smart 2007b; Whitaker et al., 1994). Whilst these controls can only be inferred for ancient platform systems, outcrop studies and seismic imaging provide considerable insight on the architectural evolution of carbonate platforms. Specifically, integration of seismic- to microfacies-scale data sets may improve the definition of 1) the different sub-environments of deposition on a carbonate platform and their distribution and nature, and 2) the carbonate factories which populate these sub-environments and their changes through time. The diagenetic history of carbonate successions can be reconstructed by the integration of different approaches, such as microfacies studies, cathodoluminescence, stable isotope geochemistry and fluid inclusion data.

The complex process of integrating information from studies of modern and ancient carbonate systems can be facilitated by a quantitative approach to the study of carbonate facies. More specifically, the development of algorithms for forward modelling of carbonate sediment production, transport, accumulation, and diagenesis provides a framework for testing the suitability of studies on modern carbonate systems to the geological record, starting from a uniformitarian approach on

the definition of the environmental (biotic and abiotic) processes. Stratigraphic forward modelling is thus a powerful tool to test conceptual models that can support the interpretation of seismic profiles (Eberli et al., 1994) or improve our understanding of the interplay of different factors, such as sea-level fluctuations, in controlling the stratal architecture and depositional patterns in carbonate platforms (Warrlich et al., 2002; Burgess et al., 2006; Paterson et al., 2006; Williams et al., 2011; Burgess, 2013). We have only recently begun to explore the potential for evaluation of coupling between sedimentology and early diagenesis (Paterson et al., 2008, Garcia-Fresca et al., 2012; Xiao et al., 2013; Whitaker et al., 2014, Frazer et al., 2014). Stratigraphic forward modelling is able to generate predictive models of carbonate platform stratigraphies that are also useful in the exploration of hydrocarbons (Boylan et al., 2002; Warrlich et al., 2008).

Forward models can be useful to test and evaluate potential interactions among different controlling parameters (as a numerical sandbox in which to understand “what happens if...?”) or to simulate real case studies (“which parameters do I need to simulate this real carbonate system?”). In this latter case, modelling should be preceded by the careful definition of the required parameters (constrained by field and laboratory data), and to withstand a robust evaluation process. Forward modelling packages produce synthetic models, which include quantitative data on the geometry, size, facies composition and distribution, and diagenetic history which may then be compared with the real case, allowing testing of the model parameterisation and their interactions. However, models always retain properties which may limit their ability to mimic real systems, their results may be affected by the processes included, computational algorithms used, temporal and spatial scale of discretisation and uncertainties in parameterisation and other input data. Thus, whilst the idea that models can ever be proved or validated is substantially wrong (Konikow & Bredehoeft; 1992), they can be tested and invalidated, and therefore represent a useful tool for quantitative evaluation of conceptual models.

In this study we develop an iterative workflow able to derive, from field and laboratory data, the parameters needed to produce a numerical model mirroring a real platform. We illustrate this workflow using the test case of the Triassic Esino Limestone succession (Casati & Gnaccolini, 1967; Jadoul et al., 1992; Berra, 2007; Berra et al., 2011) of the Pegherolo Massif, Central Southern Alps of Italy. Excellent exposures of the Esino Limestone, well preserved despite the contractional deformation, allow reliable determination of the geometry of the platform, facies distribution and composition, generation of accommodation space, and diagenetic history.

2 Forward modelling: methods and workflow

The process-based forward model CARB3D+, developed by the University of Bristol and Royal Holloway University of London was used to simulate the Esino Limestone carbonate platform. The code is able to generate 3D stratigraphic models (Paterson et al., 2006) and to simulate diagenetic processes (Paterson et al., 2008; Frazer et al., 2014). The effect of depositional and diagenetic processes can then be evaluated quantitatively by simulating fluid flow through these synthetic strata (Whitaker et al., 2014).

CARB3D+ is a process-based 3D forward simulator designed to model sedimentary facies, geometries, and early diagenesis of isolated carbonate platforms in a sequence stratigraphic context, where intrabasinal productivity is the only source of sediments (Fig. 1). It is the development of an earlier coupled 2D sedimentological and diagenetic simulator (Whitaker et al., 1997, 1999). The 3D forward modelling package differs from the 2D version in employing an explicit simulation of the evolving hydrodynamic environment and sedimentary processes, and in the incorporation of an explicit 3D model for the distribution of hydro-zones and geochemical potential to determine the diagenetic processes occurring and their rates. Depositional facies, mineralogy, and primary porosity and permeability are predicted for sediments deposited in each time step, whereas diagenetic (e.g. cementation, dissolution) and post-depositional effects (e.g. compaction) are re-calculated at each consecutive time step. Importantly, CARB3D+ includes dynamic feedback between platform morphology and sediment production and transport, as well as between sediment properties and the hydro-zones which determine the distribution of diagenetic processes. Diagenesis modifies depositional mineralogy, porosity and permeability. Additionally, porosity and sediment thicknesses are modified by early burial compaction. Porosity loss can be simulated as a function of depth of burial (diagenesis “off”) or coupled with progressive cementation through time (diagenesis “on”).

Model output is a 3D volume with data stored in cells with horizontal dimensions specified by the user, and calculated from accumulation rate during time steps of specified duration. This volume can be interrogated using displays attribute in cross-sections, well logs, single points on the cross sections, maps, and chronostratigraphic plots (Fig. 1c). Orientation of cross-sections and position of well logs are user-defined (Fig. 1b). For 3D visualization, data can be exported and displayed in other software packages.

Complex parametrization demands an optimized workflow for forward modelling. The workflow we propose is shown in Figure 2. We identify a hierarchy of parameters, ranked in terms of the confidence with which values can be assigned. Where possible, these are defined specifically for the field site (e.g., initial surface for carbonate deposition). Unknown parameters are constrained by data from modern processes (e.g. rate and depth dependence of carbonate production), or from present day conditions (e.g., for climate-related parameters). Maximum rates of sediment entrainment are set simply so that they are equal to or larger than the maximum sediment production rates in order that all the carbonate produced is potentially capable of transport under high energy conditions. When relative values or ratios among certain group of parameters (e.g., a ranking of maximum production rates for different factories) or when a range of potential parameter values was defined, a sensitivity analysis have been performed. In this way, the output of the model is assessed relative to specific test properties for the expected range of parameter values in order to identify the best value for each parameter.

It is also important to differentiate field data used to parameterise the model from field data used to test model output. To parametrize the model, detailed sedimentological studies are required, whereas the comparison between the sediment texture, provenance and diagenesis in the actual platform and in the model are fundamental to accept the output. A first test that can be readily assessed during the model run is the convergence between the observed and synthetic platform architecture. The second test is represented by comparison between the distribution of depositional and diagenetic properties observed in the real case and their distribution in the simulated platform. This is a critical test because facies in CARB3D+ are generated by the relative productivity of several separate carbonate factories, mediated by sediment transport and re-deposition. If the results of the tests are not satisfactory, the model is re-run after the identification of critical parameters and the definition of new values for them. This process continues until there is convergence between model and field data.

It should however be pointed out that similar geometries can be obtained from different sets of parameters. Given the complexity of sedimentation processes, different combinations of parameters may produce similar architectures, so that output models are thus non unique. Thus, honouring the geometry of a platform is not enough to validate a model; composition and diagenesis need to be satisfactorily reproduced. To evaluate the model, each parameter needs to be checked, to verify that all the used values are acceptable and mutually consistent, in order to avoid a model that resembles the real data but is based on unrealistic underlying parameter values.

The procedure outlined in figure 2 was followed to obtain the best estimate model presented here. At first, a range of parameter values based on data sources was used, eventually converging on a set of parameters values that returned what we judged to be the most satisfactory model. Then, a “fine tuning” of parameters was performed, until we achieved a final model able to satisfy the field and laboratory observations and data.

3. Geological setting

The Ladinian to Early Carnian succession of the Italian Southern Alps is characterised by the presence of thick, high-relief carbonate platforms separated by basinal troughs and seaways (Fig. 3). The Ladinian carbonate system developed in a greenhouse period at a paleolatitude of about 18° north (Brack et al., 1999). The flat-topped Esino Limestone, up to 700-800 m thick, consists of platform interior facies rimmed by narrow reefal and shoal facies that pass laterally to clinostратified slope breccias (Jadoul et al., 1992; Berra 2007) that prograde and interfinger with a basinal succession. (Fig. 4). The basinal deposits coeval with the Esino Limestone begin with the deposition of marly limestones (Prezzo Limestone) and nodular cherty limestones (Buchenstein

Formation). Volcanoclastic sandstones (Wengen Formation) interfinger with resedimented dark bedded limestone (Perledo-Varenna or Pratotondo Limestone).

The high-relief, flat-topped carbonate platform of the Esino Limestone shares several architectural similarities with other well-studied platforms in the geological record, such as the Carboniferous platforms of Spain (e.g., Della Porta et al. 2003, 2004) and Kazakhstan (Weber et al., 2003) or the partly coeval platforms of the Dolomites (e.g., Keim & Schlager; 1999, 2001; Marangon et al., 2011). Despite morphological similarities, sedimentological data indicate major differences between the Esino Limestone and the coeval platforms of the Dolomites and the similar Carboniferous platforms. In the Esino Limestone, microbial communities (associated with corals) are extremely important in the reef area, whereas their role decreases rapidly with depth. The slope typically comprises reef-derived breccias with clasts of early-lithified microbial limestones deriving from the reef belt. No evidence of significant microbialite production at depth higher than a few tens of meters is documented. Therefore, microbial production in the Esino Limestone was likely limited to the photic zone, with the maximum contribution at shallow water depth. This situation is different from that described in the Dolomites, where microbial production extends to 250-300 m of water depth along the slope. The slopes of the Esino Limestone are different from those of the coeval and Carboniferous platforms: they consist of breccia, characterized by a grain size distribution (coarser at the top of the slope, finer at the base) that is indicative of margin collapses (Berra et al., 2011). The carbonate factory of the Esino Limestone is thus partly different from that of other high-relief Carboniferous (e.g. Della Porta et al., 2003; 2004; Kenter et al., 2005) or Triassic (Keim & Schlager, 1999; 2001; Marangon et al., 2011) carbonate platforms. In these platforms, microbial production characterizes also the slope below the photic zone, up to more than 300 m of water depth.

Around the Ladinian-Carnian boundary (probably Early Carnian, Balini et al., 2000), a major sea-level fall produced extensive karst, paleosols, collapse and residual breccias at the top of the Esino Limestone ("Calcare Rosso", Assereto et al., 1977; Assereto & Kendall, 1977; Assereto & Folk, 1980; Mutti, 1994; Berra, 2007; Berra, 2012).

Our study focuses on the Pegherolo Massif (Fig. 3, 4), where the original depositional architecture is well preserved, from the beginning of the progradation of the carbonate platform to its demise (Berra et al., 2011).

3.1 Depositional architecture

The onset of carbonate production in the Late Anisian followed a major sea-level rise represented by the drowning of the shallow-water carbonate factory of the Camorelli Limestone and the deposition of the basinal, ammonoid-rich Prezzo Limestone (Gaetani et al., 1998; Berra et al., 2005). The Esino Limestone, subject of this study, is characterized by a first stage of aggradation followed by a rapid progradation of slope breccias over nearly 4.5 km in about 5 Ma (Berra et al., 2011). During this stage, the progradation/aggradation ratio increased from 1:1 to about 10:1.

The slope facies, mostly clast-supported breccias (Fig. 4), form a prograding margin with planar clinofolds (following the classification of Playton et al., 2010), with an angle of 35° in the upper part of the slope. The slope angle decreases toward the toe, where the profile is nearly tangential (low-angle downlap) and the distal slope facies (fine-grained breccias) interfinger with bedded basinal calciturbidites. Shelf-to-basin relief was a few tens of meters during the nucleation stage and reached in the study area 500-600 m during the progradation stage.

Slope breccia deposition occurred as mass flows probably triggered by margin collapses (e.g. Cook et al., 1972), prograding basinward. A similar origin for slope breccias has been suggested for coeval greenhouse platform facies in the Dolomites (Harris, 1994; Maurer, 2000), as well as for the icehouse Carboniferous platforms of western Kazakhstan (Tengiz oil field, Weber et al., 2003). However, Blendinger (2001) proposes translational sliding and diagenetic modifications of automicrite slopes as the controlling factors producing the steep slopes of Ladinian platforms in the Dolomites. Production of breccias in the Esino Limestone was favoured by widespread early cementation of reef and slope facies, as documented both by cathodoluminescence and stable isotope geochemistry (Frisia-Bruni et al., 1989). The development of a rigid framework in the reef and upper slope was favoured by the dominance of *Tubiphytes*, able to build steep slopes in most of the photic zone (Schmid, 1996), and microbial bindstone. The observed distribution of the

carbonate-producing microbial biota indicates the highest production in the first few tens of meters of water depth (Berra et al., 2011), whereas the rest of the slope is dominated by resedimented breccias. In the basin, the transition from the aggrading and prograding stage to the purely prograding stage is reflected by thicker resedimented carbonates, reflecting an increase of sediment supply from the platform. The cherty limestone (Buchenstein Limestone) is covered by well-bedded calciturbidites (supplied by the platform top during the progradation stage; Perledo-Varenna Fm.), with the local presence of siliciclastics (Wengen Formation) close to active volcanic centres (Fig. 4). The end of slope progradation was synchronous with the subaerial exposure of the platform top and is marked by *terra rossa* deposits on the top of the Pegherolo massif (Calcarea Rosso; Assereto et al., 1977; Assereto & Kendall, 1977; Assereto & Folk, 1980; Mutti, 1994; Berra et al., 2011; Berra, 2012).

3.2 Facies Distribution and Sediment Production

Figure 4 illustrates the stratigraphic architecture and representative facies distribution along a 4 km south-north platform-to-basin transect. This reconstruction presents the depositional architecture that should be honored by the numerical model and the different facies belts of the carbonate platform. For each facies belt, outcrop and petrographic analyses were conducted to determine sediment composition and source, as well as the sedimentary processes responsible for its deposition, in order to constrain productivity and transport parameters required by CARB3D+ (Tab. 1).

Platform interior facies (Fig. 5) are characterized by a cyclic association of a) bioclastic packstone and grainstone (occasionally associated with wackestone and, less frequently, mudstone) containing dasycladacean algae, bivalves, gastropods, foraminifera and rare brachiopods, b) oncoidal rudstone and, less frequently c) microbial boundstone. The major source of sediments is skeletal fragments, with a contribution from microbial communities. From the abundance of green algae, we infer that carbonate production was depth-dependent, with a maximum production in the shallowest part of the water column.

Shoal margin facies (Fig. 6) are massive and consist of sand-size, high-energy deposits. They are composed of bioclastic to intraclastic grainstone/packstone to fine rudstone, containing bivalves, gastropods, echinoids, crinoids and foraminifera. The type of skeletal grains reflects production in a high-energy, shallow-water setting.

Reef facies (Fig. 6) are dominated by microbial boundstone (*Tubiphytes* and, occasionally, corals, which become more common during the progradation stage) rapidly passing basinward to slope facies. Large growth-framework cavities are filled by isopachous fibrous radial calcite, typically observed in reef facies (e.g. Davies, 1977). The reef facies are preserved as a narrow belt that rapidly passes seaward to massive slope breccias. The sharp transition from reef to slope breccias suggests a high carbonate production in the first few meters of water depth. Production also occurred at depth, as documented by the presence of microbial associations and *Tubiphytes* (Schmid, 1996).

Slope facies (Fig. 6) are almost exclusively represented by clast-supported, mud-free, reef-derived breccia, with some indication of sparse *in-situ* production, represented by automicrite and microbial mats within the breccia clinoforms. Intergranular porosity is filled by different generations of calcite cements. In the slope facies, carbonate grains from the platform interior and from the shoal margin are scarce suggesting sediment bypassing the steep slopes. Thus, slope facies of the Esino limestone are mainly derived from the downslope transport of reef-derived carbonate breccias, with a minor contribution from *in-situ* production by microbial carbonates directly produced along the slope.

Basinal facies (Fig. 6) are dominated by thinly-bedded mudstone and wackestone with normal grading and parallel lamination. Basinal limestone is mainly represented by resedimented intraclastic-bioclastic packstone to wackestone, as carbonate pelagic contribution to sedimentation is negligible to absent in the Middle Triassic. Sediment composition indicates that basinal limestones are the product of the resedimentation of sediments produced on the platform top. These sediments bypassed the steep slope and were deposited at the toe of the prograding platform, where they interfinger with the most distal part of the clinoforms.

4. Model parameterization

CARB3D+ requires five sets of parameters (here described) for sedimentological simulations, with an additional set of parameters required to model diagenesis (Tab. 1). Initial topography, can be defined reasonably well by careful study of outcrops or analysis of seismic data. Carbonate production parameters may be deduced from sedimentological and paleoecological analysis. Parameterization for diagenetic processes is more challenging, and based on the identification and characterization of the different diagenetic events, with particular attention to the early-diagenetic phenomena.

4.1. Model duration and time resolution

The focus of this study is the evolution of the Esino Platform from the Late Anisian to the Early Carnian. The duration of the Ladinian (International Commission on Stratigraphy) is about 5 Ma, that is considered the time interval for our model. With a 5 Ma time interval, the time resolution is critical as a high temporal resolution may lead to excessive calculation times, whereas a lower temporal resolution may not adequately account for the effects of high-frequency sea-level oscillations on sedimentation. Sensitivity analyses identified an optimal calculation increment of 4 ka, because it resulted in a run time short enough that multiple scenarios can be simulated (about one week for each complete model) and at the same time provided a sufficient number of sampling points along the high-frequency sea-level curves used in the model.

4.2 Model domain dimensions and initial platform geometry

Geometric parameters are necessary to define the areal extent of the model domain, its spatial resolution and the initial depositional surface. The Esino platform prograded to both north (well preserved) and south (poorly preserved), giving a total platform width of approximately 18 km. A domain including the entire platform (about 25 x 25 km) at a spatial resolution required to capture the detail of the platform growth would have resulted in unreasonable computing time. Therefore, only the northern half of the platform was considered in the simulation (Fig. 2). As the initial geometry at the nucleation stage is unknown, we used a circular nucleation center with a radius at the top of 2.5 km. Modelling a smaller platform reduces the platform interior area that sources part of the basinal sediments, potentially impacting the gross sediment production available in the model. However, field observations suggest that the slopes were fed predominantly by the reef and uppermost slope, with most platform interior sediments delivered to the basin and bypassing the slope. Thus, the deficiency in gross sediment production is likely to be minor. Sensitivity analysis suggests that the size of the platform, and thus the area of the platform interior, does not have a significant impact on the architecture of the northern progradational side of the platform. A critical parameter for the model calculation is the grid resolution. In our model, the existence of narrow reef belts forced definition of the spatial resolution of the grid size at 100x100 m, representing a pragmatic balance between the required resolution with a manageable model run time.

Field observations indicate that the platform-to-basin relief was initially approximately 200 m. At the end of the studied time interval the platform-to-basin relief had increased to 500-550 m, with a total thickness of platform facies of about 800 m above the nucleation zone (Berra et al., 2011). The final geometry of the platform is characterized by clinostatified slopes (up to about 35°) and toplap. The progradation is about 4 to 5 km. In order to avoid boundary effects, a model domain of 15x15 km was used.

4.3 Accommodation

Accommodation in CARB3D+ is controlled by three interacting parameters: eustasy, subsidence and surface dissolution during periods of platform exposure. Eustatic sea-level variations are simulated using a composite curve comprising three sinusoidal sea-level curves of user-defined frequency, magnitude and asymmetry. This cyclicity is superimposed on a longer-term trend in subsidence/uplift, which may vary spatially. Surface lowering by dissolution is controlled by rainfall, both as a direct function of flux and, indirectly, via its effect on vegetation and soil (Whitaker & Smart 2007a). The generation of accommodation space is offset by net sediment accumulation, determined from the rates of *in situ* sediment production, deposition of transported sediment, subaerial dissolution and submarine erosion.

Accommodation space in the model is controlled by the relative sea-level curve, which includes 2 components: cyclic eustatic curves of different frequencies and amplitudes (Goldhammer et al., 1990), and a longer-term subsidence component. Accommodation space is further generated by surface lowering due to dissolution of the platform top during subaerial exposure. The modeled accommodation must account for the 700-800 m thickness of the Esino Limestone, whilst the transition from aggradation to progradation and the toplap geometry suggests a decrease in subsidence through time. This trend culminates in the prominent subaerial exposure at the top of the Esino Limestone, ascribed to a major eustatic sea-level fall (Mutti, 1994), by an estimated 20-30 m (Berra et al., 2011).

The amplitude of the high-frequency sea-level cycles (Goldhammer et al., 1990) varies significantly according to global conditions (i.e. greenhouse vs. icehouse). High-frequency sea-level cycles are recorded in the platform interior of the Esino Limestone by shallowing-upward cycles (from about 0.3 to 1.5 m thick) comprising a subtidal, bioclastic to oncolitic unit capped by a stromatolitic layer (Fig. 3). The cycle boundary is defined by a transgressive surface, with little evidence of sub-aerial exposure or erosion at the cycle top, suggesting a low amplitude (dm, at most m scale, compatible with greenhouse conditions, Schulz & Schäfer-Neth, 1997) for the observed high-frequency sea-level changes.

In order to calculate the average duration of each cycle we measured two stratigraphic sections in the platform interior, one in the aggradation stage and one in the progradation stage. Fischer Plots (Fig. 3, no correction has been applied for compaction on field data) show that the average thickness of the cycles in the lower aggrading part of the platform is 104 cm (for 42 measured cycles), reducing to about 30 cm (45 cycles) in the upper progradation stage, where peritidal facies are more common. The number of cycles in the platform interior facies of the Esino Limestone is between 700-800 (all thicker cycles) and c.2500 (all thinner cycles). Considering the thickness of the Esino Limestone and the number of cycles (even if considering no missed beats), the average duration of the cycles results sub-Milankovian, in agreement with values reported for other Triassic platforms in the Tethyan realm (Schwarzacher & Haas, 1986, Reijmer et al., 1991; 1994; Zühlke et al. 2003; Mundil et al., 2003;). To simulate the observed stacking pattern of the platform interior facies we have added a high-frequency asymmetric sea-level curve (frequency: 5 ka). The amplitude of this highest-frequency sea-level oscillation was set at 0.5 m, compatible with a greenhouse context as the Middle Triassic.

A Milankovian cyclicity of 20 ka (precession) and 100 ka (eccentricity) years has been also added. The absence of dissolution and karstic features at the top of the possibly 20 ka cycle sets suggest that amplitude of this cyclicity was reduced (we use 3 m), reducing surface lowering. For the 100 ka cycles (poorly recognizable) we use an amplitude of 1 m.

The duration of the highest-frequency cycles is important for the definition of the time-step of the model calculation, which needs to be significantly shorter than the duration of the cycle. Model run time using time steps of 1 ka were excessive, the smallest time-step commensurate with reasonable run time (one week) has been identified in 4 ka. The 4 ka time step resulted the best compromise as i) the calculations with the 4 ka time step was borne by the hardware (the time step of 1 ka precluded simulation for a total time of 5 Ma) and ii) facies variability in the shortest simulated cycles (20 ka) was mimicked in the model.

4.4. Sediment production

Carbonate sediments are produced in four separate factories: reef and shoal margins (characterized by different wave energy conditions), platform interior, and the pelagic realm. Production rates of pelagic sediments are low and independent of water depth. The relative contribution of the different carbonate factories to sedimentation has been inferred from the sediment composition and depositional processes, thus ranking the production rate of each carbonate factory, as well as providing constraints on how much of the produced sediments is transported and re-deposited. For reef, platform interior and marginal sediments, production can be specified as a function of water depth. The ratio of interior to marginal production varies with restriction (affecting hydrodynamic energy), which increases with distance from the open ocean. CARB3D+ considers two sediment types: granular (non-cemented) sediments, and boundstones (reefs) that are cemented on deposition. Granular sediments are further subdivided into coarse grains (here defined as 0.5 mm grain diameter) that are produced at shoal margins and fine grains (0.063 mm diameter) that are produced in the interior and pelagic realms.

Coarse and fine sediments are produced *in situ*, but a fraction of these are suspended by the shear stress generated by the orbital velocity of the waves, and by currents. Once a critical shear stress is exceeded for a given particle size, the rate of entrainment increases with increasing velocity. In CARB3D+, transport of sediments from their site of production to the site of deposition is driven predominantly by currents; when current velocities fall below the critical threshold for fine sediments, deposition occurs at a rate determined by the settling velocity and water depth. For coarse sediment, the rate of deposition is determined by the slope angle and current speed and direction. Reefal sediments are subject to a user-defined degree of bio-erosional processes and are then available for sediment transport.

Slopes in CARB3D+ are considered to be angle-of-repose slopes (Kenter, 1990). Where the slope angle exceeds the angle of repose (controlled by the percentage of fine sediments in transport), deposition cannot occur and sediment is moved downslope until the critical angle of repose is not exceeded. Where boundstones are deposited, the critical angle of repose is assumed to be 90° due to the ability of some reefs to grow ocean-facing vertical walls (Read, 1985; Grammer & Ginsburg, 1992).

Facies are defined in CARB3D+ using a modification of the Dunham (1962) classification as: boundstone (>50% reefal component) and, from the texture of the granular component, as grainstone (< 10% fine), packstone (10–30% fine), wackestone (30–90% fine), and mudstone (>90% fine). Depositional porosity is reduced by compaction on the basis of data for non-cemented carbonate sediments summarized in Goldhammer (1997), and is dependent on the coarse: fine ratio. Compaction of boundstones is assumed to be negligible. Sequential simulations of the hydrodynamics and sedimentology are performed at specified time steps.

Sediments generated by the four factories modelled by CARB3D+ are subject to transport and deposition (Fig. 7), resulting in the formation of various facies (Hubbard et al., 1990). The interplay between carbonate production and sediment transport controls the geometry, facies composition and internal architecture of the simulated platform.

The maximum production rate, the production-depth distribution curve and the coarse-fine ratio of the sediment have been defined for each of the four carbonate factories, the preferred values for these parameters have been defined through sensitivity analyses.

The absence of any siliciclastic sediments during limestone deposition in the study area suggests that waters were likely to have been clear, and thus the rate of light reduction with depth has been defined as low, causing a slow decrease of carbonate production with depth. In both interior and margin factories, the presence of green algae suggests that sediment production occurred in persistent shallow water settings. The abundance of bioclastic deposits in the margin area indicates a higher production with respect to the interior (Tab. 2). The values for interior production used in the model are slightly lower than those calculated for the Bahamas by Demicco and Hardie (2002) and Broecker and Takahashi (1966) and in the range of those reported by Enos (1991). High productivity is required for the reef factory as the platform slope clinofolds (representing a large volume of the Esino Limestone) are composed predominantly of reef-derived sediment. Framework growth rates in the Holocene Great Barrier Reef up to 16 m/ka, with a modal value of 7-8 m/ka (Hopley et al., 2007 and references therein). We adopted a maximum production rate of 8 m/ka, comparable with these values. Smith and Kinsey (1976) propose for modern coral reefs a productivity between 3 and 5 m/ka, but the later are time-averaged mean accumulation rates (thus, expected to be lower than the actual production rate; Schlager, 1999). Higher values are reported by Enos (1991).

Microbial contribution to carbonate productivity is high in the reef area (Berra et al., 2011), but it rapidly decreases at depth. Although there is evidence for some *in-situ* production by microbial carbonates on the slopes, this is limited in comparison with the volumes of carbonate shed from the shallow slope-reef belt. This situation marks a significant difference of the Esino Limestone in comparison with other high-relief, steep-slope carbonate factories similar for geometry (e.g. Sierra de Cuera; Della Porta et al., 2002; 2003; 2004) or for age (e.g. carbonate platforms of the Dolomites; Keim & Schlager, 1999; 2001; Marangon et al., 2011). To simulate the greater production at depth of the microbial-rich reefs, compared to present day coral reefs, we set the depth for maximum reef production at 8 m (Tab. 2) with a decrease with depth more gradual with respect to present-day reefs. In order to reflect the continuous failure of the reef margin producing the slope breccias, the production area for the reef factory was set narrower than that for margin sediment production (reef: 0.5 km; margin 1.2 km). Apart from a few groups of pelagic bivalves, the

skeletal contribution to the pelagic realm was virtually nil during the Triassic. Nevertheless, to simulate the contribution to basinal sedimentation from the suspension of fine-grained carbonates from the adjacent carbonate platform, it has been set to a very low value (0.001 m/ka).

4.5. Paleocceanographic parameters and sediment transport

Sediment transport in CARB3D+ is dependent both on downslope transport and, after sediment entrainment, by waves and currents. Sedimentary observations from outcrop provide constraints on the environmental energy conditions. Coarse bioclastic grainstone/rudstone in the platform margins and, less frequently, in the platform interior document high-energy conditions, with loss of fines to the deeper basin. Wind speed values (Tab. 2) can be obtained from modern tropical settings, but a number of tests are required to determine which wind speed results in a realistic amount and distribution of sediment transport. Wind speed of 15 m/sec (winds up to 19 m/sec are documented in the Caribbean, Altai & Farrugia, 2003), and maximum current velocity at the model boundary of 0.2 m/sec (comparable with the data by Fratantoni, 2001) have been considered. Comparable values are reported also for the Bahamas (Bergman et al., 2010) and Belize (McNeill et al., 2010). As wind and current strength and direction varies, often in a systematic manner, during the year and even over longer time scales CARB3D+ allows the incorporation of some variability in both the current and wind directions. We set both as $\pm 30^\circ$. Wave friction coefficient and sediment entrainment rates have been defined after a wide range of sensitivity tests, as they could not be constrained with sedimentological analyses.

Much of the platform slope is composed of breccia, derived from the upper slope and margin through mass wasting. This mechanism poses a specific challenge, as breccias cannot be explicitly simulated in CARB3D+, neither in terms of production processes (e.g. reef-upper slope collapse) nor downslope transport and distribution. At present routines in CARB3D+ to simulate failure of the over-steepened slopes and breccia production are still under development (Flory et al., 2014). To simulate breccia deposits comparable to breccias in terms of source area, texture and depositional processes, a rigid framework of reef/upper slope facies is required, together with an efficient process to move carbonates from the reef area to the slope. We obtained a rigid framework for the reef/upper slope deposits in the model by increasing the percentage of boundstone in the reef factory. The collapse of most of the reef and part of the upper slope facies was simulated using the bioerosion function, in CARB3D+. This produced large volumes of coarse sediment, which was re-worked downslope by grain avalanching, and deposited at angle of repose.

4.6. Diagenesis

CARB3D+ simulates both marine and fresh-water diagenesis. The diagenetic component of CARB3D+ includes prediction of the spatial and temporal distribution of hydrozones and tracking of cumulative residence times for sediments within these zones, taking into account sea-level, effective rainfall (rainfall minus evapotranspiration) and sediment hydraulic conductivity. Within meteoric hydrozones, diagenetic processes (mineral stabilisation, dissolution and cementation) are distributed according to a set of rules based on climate and soil development. In the case study, diagenesis is exclusively marine, as deduced from field and laboratory data.

CARB3D+ algorithms allow simulation of early diagenesis through the definition of a set of parameters including (a) the primary carbonate mineralogy (abundance of primary aragonite and calcite) for the four carbonate factories (platform interior, margin, reef and pelagic) and the rates of (b) cementation and (c) dissolution in four diagenetic hydrozones (freshwater vadose and freshwater phreatic, mixing and saline zone). Permeability is calculated by CARB3D+ from sediment texture and porosity based on the approach of Lucia (2007).

Based on the types of skeletal grains, we have set the calcite/aragonite ratio for the platform interior and the pelagic factories at 3:7 (Tab. 2). The calcite/aragonite ratio for the platform margin and the reef factories has been set to 1:1 to account for the lack of typical aragonitic precipitates. Aragonite and high-Mg calcite were the primary inorganic calcium carbonate precipitates in Triassic seas (Stanley & Hardie, 1998), in agreement with the data by Frisia-Bruni et al. (1989) who indicate an original aragonitic or high-Mg calcite mineralogy for the cements of the Esino Limestone.

Rainfall rate is an important parameter as it controls subaerial dissolution, soil development and occurrence of meteoric groundwater beneath a fresh-water table. As mean annual rainfall (and

evapotranspiration) are difficult to constrain from the fossil record, they can be partly deduced from paleoclimate simulations available for the time of interest (Sellwood & Valdes, 2006) or from appropriate modern analogues. During most of the Triassic the climate of the Tethys was arid (Kutzbach & Gallimore, 1989). A low rate of surface lowering (15 mm/ka) and a high evapotranspiration rate (up to 90% of rainfall) was used. These values are based on modern studies of bare limestone surfaces in semi-arid to arid environments and islands with very thin vadose zone (Moses et al., 1995; Whitaker & Smart, 2007b), and evidence of significant carbonate recycling during exposure (Miller et al., 2012). Evidence of meteoric diagenesis (vadose cements, paleosols and karstification) is restricted to the Calcare Rosso (Assereto & Kendall, 1977; Mutti, 1994) which is interpreted as deposited during a fall in relative sea-level and a possible shift to more humid climate conditions (Mutti, 1994; Berra, 2007; 2012). This climatic change marks the end of the platform growth and was not modelled in our study.

The dominance of marine cementation observed in outcrop further constrains simulations of diagenesis mostly to the saline zone. Pore-filling events have been reconstructed by petrographic analysis of thin sections under polarized microscope and cathodoluminescence, which indicate a common diagenetic evolution for the entire platform, with no differences in the aggrading and the prograding stages. Moreover, pores of different size and from different platform sub-environments (interior, margin, reef and slope) share a common cement stratigraphy, although the abundance of cements differs substantially. Large reef growth framework porosity (up to few dm), slope breccia interparticle porosity, and small intra- and interparticle pores (mm) in grainstones from the platform margin are filled almost completely by non-luminescent, isopachous rims of radial fibrous calcite occasionally with scalenohedral terminations. Inorganic geochemical studies support the marine origin of these cement rims (Frisia-Bruni et al., 1989). Late burial, orange-luminescent equant calcite and, locally, dolomite occluded the remaining porosity (Fig. 8).

In the coarse-grained facies, marine cements represent up to 35-40% of the rock. The majority of cements precipitated shortly after deposition (Berra & Carminati, 2012), and reduced the initially high primary porosity to values between 3 and 5%. Sensitivity tests suggest that a similar rapid reduction of primary porosity can be achieved with a saline cementation rate in marine pore waters, set at 0.2% Total Rock Fraction/ka (Tab. 2). Cementation rates comparable with those used in the model are described in present-day platforms (Grammer et al., 1999).

5 The numerical model: discussion of the results

Hundreds of developmental runs have been undertaken to tune the different parameters in order to produce a best-estimate, site-specific model able to honour field observations. Different combinations of controlling parameters have been tested to evaluate their relative effect and interactions by a constrained sensitivity analysis process. The sensitivity analyses showed that different combinations of productivity and accommodation curves, wind speed and entrainment rate (being these the most critical parameters in our model) produced completely different final architecture and facies distribution, with a non-linear interaction of these parameters. Once a combination of parameters selected in the range defined by field data was able to produce a model resembling the field situation, a fine tuning was performed until a satisfactory model was obtained. The best-fit model, reported in Figure 10 and subsequent figures, has been compared with the field and laboratory data, in order to test its coherence and to verify a satisfactory simulation of different sedimentological aspects (e.g., sediment source and texture, petrophysical properties, diagenetic history, facies distribution) recognized in the field, discussing possible critical aspects. In particular, the matching with the field data of the platform architecture together with the facies distribution in the model has been considered the most important parameter to test the modelling results.

5.1 Sensitivity analyses: interaction of parameters

Sensitivity analysis provides an important tool to test the effects of changing sets of parameters. Figure 9 presents a matrix of results of one example of sensitivity analyses, performed using two wind speeds and three production rates for the reef and margin factories. The ratio of reef-to-margin production is maintained at 2:1 in all runs, in agreement with field observations. At the lower wind speed (Fig. 9 a,b,c), sediment entrainment is limited to a narrow zone adjacent to the windward margin of the platform. There is therefore little sediment shed from the platform edge and progradation is limited. At the highest considered carbonate production rate (Fig. 9 c,f), the

progradation is lowest because production is limited by the shallow water depth on the platform top.

None of the low wind speed simulations shows much similarity to the actual platform because insufficient sediment is generated and shed from the platform margin to drive progradation. At higher wind speed, much more sediment is entrained and shed downslope from the platform margin. No linear relation between maximum sediment production and progradation has been observed in the model. A combination of wind speed and productivity controls the progradation rate in a complex manner: for the lowest wind speed, the lowest progradation is obtained with the highest production rate, whereas for the highest wind speed, the lowest progradation is obtained with the lowest production rate.

In addition to the depositional architecture, there are significant differences in the facies present with variations in wind speed. With the lower wind speed (Fig. 9 a,b,c), much more reef is preserved in the simulations than is observed in the field, a direct result of the low energy conditions. In contrast, with the higher wind speed, much less reef is preserved, and there is a systematic pattern of increasing preservation and downslope extent of the reef at progressively higher production rates. It is noteworthy that at the high wind speed and at lower carbonate production rates, facies in the platform interior develop channels and a larger amount of margin facies. At the highest production rate, the reef facies are more abundant. Of the 6 simulations shown in Figure 9, the one with a 15 m/s wind speed and production at 8 m/ka in the reef and 4 m/ka in the margin is the closest to the architecture and facies proportion observed in outcrop (Figs. 2; 10). These rates are therefore adopted for the final simulation (Tab. 2).

5.2. Geometry and facies distribution

Geometry and facies distribution observed in outcrop have been compared with those obtained for the windward side of the synthetic platform (Fig. 10).

In the CARB3D+ model, we used a dominant wind, which produced strongly asymmetrical platform margins and different basinal successions on the leeward and windward sides of the platform (Fig. 9). The prevailing wind direction during accumulation of Esino Limestone cannot be deduced from field data, because only one side of the platform is well exposed and the potential asymmetry of the platform cannot be evaluated. However, the best match of the field data was achieved for the windward side of the synthetic platform, where the progradation is an order of magnitude higher than in the leeward side. The total progradation of windward slopes of the synthetic platform is comparable with that observed in outcrop (about 3.5-4.0 km vs. about 4.5 km respectively, Fig. 10). Also in term of sediment texture, the dominance of grain-supported slope facies without fine-grained material is considered the equivalent of the slope breccias observed in outcrop, in agreement with the coarse reworked type of slopes in the digital model (Fig. 10).

The accommodation curve (Fig. 11) proved to be the most important parameter controlling the thickness of sediment accumulation on the platform and in the basin, as well as the variations in the platform-to-basin relief. As production rates for the different sub-environments of the platform were held constant over the 5 My simulated, the observed shift from aggradational to progradational architecture was mainly controlled by the relative sea-level. Analysis of accommodation curve (Fig. 11a) and the chronostratigraphic chart (Fig. 11b) reveals that the absolute progradation rate is constant for the entire simulation period and it is not affected by the reduction in accommodation rate on the platform top. Such constant rate of progradation suggests independence of production and erosion of the reef facies from accommodation. It also indicates that the increase in the area of platform interior over the course of the model run has no effect on the amount of progradation in the simulation, suggesting that the progradation is mostly controlled by reef production. Simulated and observed basinal sediment thickness, slope geometry and platform progradation in the windward side (Fig. 11) are also comparable. The chronostratigraphic chart shows that sedimentation is continuous along the slopes and in the basin, whereas hiatuses occur on the platform top due high-frequency subaerial exposure. This results in a highly discontinuous sedimentary record on the platform top when creation of accommodation space decreases, about 1.7 Ma from the beginning of the model. Thus, whilst reducing accommodation leads to an increase in the number of missed beats, platform top production rates are sufficiently high that there is no under-filled accommodation in any stage of the platform development. The digital facies distribution is controlled by productivity and sediment transport parameters. The windward margin and platform interior facies are characterized by increasing mud content toward

the centre of the platform. In the model, the propagation of wave energy decreases toward the platform interior, due to the high productivity of reef and margin shoals.

Examination of a platform-to-basin cross-section from the windward margin of the numerical model indicates that most of the slope sediment consists of coarse reworked material mostly derived from the reef (Fig. 10). Variation in total sedimentation rate along the depositional profile (solid blue line in Fig. 10d) supplies further information on sediment provenance. At the final step of the model, negative accumulation (i.e. net erosion) is observed in the narrow reef belt, suggesting that most of the sediment produced by the reef was rapidly remobilised. This result has been achieved in the model by coupling the reef production rates (defined according to field observations and sensitivity analyses) with efficient bioerosion on the reef facies, so that most of the sediment produced by the reef was eroded and redeposited along the windward slope. Consequently, the preserved reef facies belt in the model is narrow despite the high productivity. Along the slope, production is reduced but net sediment accumulation rates remain high to depths >300 m, reflecting deposition of sediments eroded from the reef along the slope. Grainstone modelled accumulating on the slope is equivalent to the observed clast-supported slope breccia, and accords with the absence of fine-grained deposits filling the intergranular space.

5.3. Diagenesis and porosity/permeability distribution

Interactions between sediment production, deposition and diagenesis are simulated at each step of the evolution of the synthetic platform. Results of the forward modelling have been tested considering compaction (both with diagenesis on and off) and cementation. Compaction and cementation are strongly related to the different facies of the digital platform and control the distribution of porosity and permeability in the platform (Fig. 12).

Compaction alone (diagenesis off) is highest in the muddy sediments of the platform interior, and decreases toward the reef and slope where porosity destruction in response to early burial is less intense. In the model, additional accommodation created in the platform interior by early compaction is rapidly filled by over-production by the platform interior factory, maintaining a flat-topped geometry of the platform.

When diagenesis is modelled, both compaction (because early cementation reduces the compactability of the sediments), and porosity decrease, due to cement precipitation in both fine- and coarse-grained facies. To simulate the observed decrease in porosity due to abundant early marine cementation, a high saline cementation rate was used (Tab. 2). This is in agreement with the high carbonate saturation proposed for Triassic seawaters in equatorial latitudes (e.g. Riding & Liang, 2005). Marine cementation simulated in the model rapidly occludes fabric-controlled porosity, in agreement with pore occlusion observed in the field due to precipitation of early fibrous radiaxial isopachous marine cements (Frisia-Bruni et al., 1989) in the mud-free slope facies and margin belt. In the field, porosity at the time of deposition of the slope breccias (evaluated removing the area of early marine and late burial cements on selected images) reaches 40% and reduces to about 3-5% (mostly due to precipitation of early marine cements; Fig. 8) before the deposition of the late burial cements (not present in our model). These values are similar to those observed in the model for the slope facies at the time of deposition and after residence in the saline zone.

Within the saline zone, the cementation rate is constant and is a function solely of residence time of exposure to supersaturated fluids. The specified rates of cementation are sufficiently rapid that almost all porosity in the coarse, mud-free slope facies is occluded within 200 ka after deposition. Efficiency of cementation is strictly related to the sediment type: cementation is uniform and extensive in the slope facies; it is less homogeneous in the platform interior, where porosity is lower due to the abundance of more compressible fine-grained sediments (Fig. 12e).

Diagenetic alteration by meteoric/brackish waters is expected on the platform top. This is particularly true of sediments deposited during the later stage of the platform evolution when accommodation was more limited and, thus, shallow sediments were repeatedly exposed. Because of the inferred aridity, dissolution is assumed to be negligible. The dissolution potential of the shallow fresh-salt water mixing zone is assumed similarly limited. Total residence time in the mixing zone is, in the model, rarely longer than about 10 ka during the aggradational stage and reaches 200 ka on the platform top during the progradational stage, resulting from the cumulative overprinting of different exposure episodes. In addition, selecting both the no soil option in the model and low recharge rate restrict rates of dissolution. The diagenetic history is, thus, dominated

by the progressive reduction of the original porosity by marine cement precipitation and sediment compaction, in agreement with field observations.

Diagenesis also impacts the distribution of permeability in the synthetic platform. Permeability is highest at time of deposition, in mud-free slope facies, but decreases significantly after cementation and compaction. In the muddy platform interior facies, porosity is significantly reduced by compaction (Fig. 12). In the backreef, coarser deposits show higher cementation volumes. The contribution of marine cements to the reduction of permeability is clearly shown by comparing model results simulating diagenesis and compaction with those simulating compaction only (Fig. 12). In outcrop, the highest values of residual porosity after marine cementation are observed in the reef area, where large cavities were not completely filled by cements. The rapid porosity loss by cement precipitation in the model agrees with field observations (Fig. 8).

6. Conclusions

Numerical modelling is an important tool to evaluate the interaction of parameters impacting sediment production, distribution and diagenesis and to simulate real case studies. In order to produce a model that mimics an existing carbonate platform, the parameters that control these processes need to be carefully evaluated and constrained. Constraints for real case studies derive from i) detailed field work on the geometry/architecture of the selected platform, ii) sedimentological study of the different facies and their distribution and associations and iii) the diagenetic history. Data not deducible from field observations, such as currents and wind direction and intensity, can be obtained with a uniformitarian approach with reference to modern analogues or paleoclimatic models and evaluated by sensitivity analysis. Constraints on the initial and final geometry and internal architecture of the models can be obtained by stratigraphic reconstructions (for outcropping succession) or seismic images (for subsurface settings). Forward modelling, thus, represents a powerful tool to integrate data from the geological record with data from present-day observations and seismic geometries, promoting the critical integration of different datasets.

The workflow we followed requires the production of a large number of simulations, which are obtained by first defining the acceptable ranges for the required parameters and then performing a detailed sensitivity analysis. Using this interactive process, a model can be tuned until there is an adequate match between the key descriptors selected to assess the model (synthetic platform geometry, nature and distribution of digital facies, porosity evolution) and those observed for the case study. The match between model and real data can be quantitatively evaluated in terms of geometry and facies distribution, and volume of cement occluding original porosity. However, defining an “adequate” match is inherently subjective. In the test process, we keep separated the field data used for model parameterisation (e.g. microfacies studies and sedimentological field data) from data used to test the numerical model (e.g. final geometry, porosity distribution, source of sediments) in order to have independent criteria for model definition and evaluation. This distinction is not only important conceptually, but also critical to the workflow followed here.

Although forward modelling software packages such as CARB3D+ inherently simplify the complexity of natural systems (e.g., not including early fractures rapidly sealed by marine cements, observable in recent; Whitaker and Smart, 1997, and ancient margins; Kosa and Hunt, 2005; Frost and Kerans, 2009, 2010; Berra and Carminati, 2012), process-based simulations enable a numerical quantitative study. The realistic ranges of the different parameters which control the development of carbonate systems may be constrained integrating data from modern and ancient carbonate systems. However, it should be remembered that models can never be proven or validated, but only “tested and invalidated” (Bredehoeft and Konikow, 2012). Uncertainties, due to the fact that parameters cannot be precisely quantified, do not undermine the utility of the approach, which still represents the best available means for synthesis, analysis and testing our understanding of the relationship between sedimentological process and their products preserved in the fossil record.

A quantitative approach to the study and modelling of carbonate systems has two major impacts: 1) provide new insights into the interaction of different parameters controlling the growth of a carbonate system and early diagenetic alteration (both applied to real case-studies or as experimental tests), and 2) provide a 3D digital numerical model that can be used for the parameterisation of the petrophysical properties of selected complex geological bodies, with potential application to georesources. When modelling focuses on specific geological situations, it

could provide important clues on the forecast of the distribution of physical properties (such as porosity, with implications, for example, on the definition of reservoir quality distribution scenarios and on the modelling of fluid flows) or help in predicting facies distribution where data are poor or missing. Nevertheless, it is important to remember that no model can ever be a perfect fit to reality and that every carbonate platform will exhibit some features unique to its individual sedimentological and diagenetic history. What we can deduce from a numerical model must be critically evaluated and continuously tested to ensure that it honours the field data. The best use of such models is thus in extending our 3D understanding of often much more limited data, for instance from a limited number of key well logs. The risk is to confuse the model with reality which, as Golomb (1968) wisely highlighted, is like “looking for oil by drilling through the map”.

Acknowledgements

This study is a part of a research project on carbonate reservoirs supported by ENI and by PRIN 2010-2011, Ministero dell'Istruzione dell'Università e della Ricerca (20107ESMX9, F. Berra). We would like to thank all those who supported our research, in different ways and at different times. Fruitful discussion on the sedimentological interpretation of the Esino Limestone facies with F. Jadoul (Milano) are acknowledged, as well as the field support by M. Binda (Milano). A former version of this manuscript benefitted from the comments of Gareth Jones and Dider Granjeon. The detailed reviews of John Reijmer and Beatriz Garcia-Fresca, as well as advice from the Associate Editor Nereo Preto are here warmly acknowledged: their constructive comments improved this manuscript considerably. Model development of CARB3D+ was carried out in collaboration with D. Waltham and colleagues at RHUL and funded via the Bristol Carbonates Consortium by Chevron, Conoco-Philips, ENI, ExxonMobil, Petrobras and Shell. We also acknowledge G. Felce (Bristol) for technical support in generating the presented results.

References

- Altaii, K. and Farrugia R.N. 2003. Wind characteristics on the Caribbean island of Puerto Rico. *Renewable Energy*, **28**, 1701–1710.
- Assereto, R. and Kendall, C.G.St.C. 1977. Nature, origin and classification of peritidal tepee structures and relative breccias. *Sedimentology*, **24**, 153-210.
- Assereto, R. and Folk, R.L. 1980. Diagenetic fabric of aragonite, calcite and dolomite in an ancient peritidal-spelean environment: Triassic Calcare Rosso, Lombardia, Italy. *J. Sed. Petrol.*, **50**, 371-394.
- Assereto, R., Jadoul, F. and Omenetto, P. 1977. Stratigrafia e metallogenese del settore occidentale del distretto a Pb, Zn, fluorite e barite di Gorno (Alpi Bergamasche). *Riv. It. Paleontol. Strat.*, **83**, 395-532.
- Balini, M., Germani, D., Nicora, A. and Rizzi, E. 2000. Ladinian/Carnian ammonoids and conodonts from the classic Schilpario-Pizzo Camino area (Lombardy): reevaluation of the biostratigraphic support to chronostratigraphy and paleogeography. *Riv. Ital. Paleontol. Stratigr.*, **106**, 19-58.
- Bergman, K.L., Westphal, H., Janson, X., Poiriez, A. and Eberli, G.P. 2010. Controlling parameters on facies geometries of the Bahamas, an isolated carbonate platform environment. In: *Carbonate Depositional Systems: Assessing Dimensions and Controlling Parameters – The Bahamas, Belize and Persian/Arabian Gulf* (Eds H. Westphal, B. Riegl and G.P. Eberli), pp. 5–80.
- Berra F. 2007. Sedimentation in shallow to deep water carbonate environments across a sequence boundary: effects of a fall in sea-level on the evolution of a carbonate system (Ladinian-Carnian, eastern Lombardy, Italy). *Sedimentology*, **54**, 721-735.
- Berra, F. 2012. Sea-level fall, carbonate production, rainy days: How do they relate? Insight from Triassic carbonate platforms (Western Tethys, Southern Alps, Italy). *Geology*, **40**, 271–274.
- Berra, F. and Carminati, E. 2012. Differential compaction and early rock fracturing in high-relief carbonate platforms: numerical modelling of a Triassic case study (Esino Limestone, Central Southern Alps, Italy). *Basin Res.*, **24**, 1–17
- Berra F, Rettori R. and Bassi D. 2005. Recovery of carbonate platform production in the Lombardy Basin during the Anisian: paleoecological significance and constrain on paleogeographic evolution. *Facies*, **50**, 615-27.
- Berra, F., Jadoul, F., Binda, M. and Lanfranchi, A. 2011. Large-scale progradation, demise and rebirth of a high relief, flat-topped carbonate factory (Late Anisian-Early Carnian, Lombardy Southern Alps, Italy). *Sed. Geol.*, **239**, 48–63.
- Blendinger, W. 2001. Triassic carbonate buildup flanks in the Dolomites, Northern Italy: breccias, boulder fabric and the importance of early diagenesis. *Sedimentology*, **48**, 919-933
- Bosence, D. 2005. A genetic classification of carbonate platforms based on their basinal and tectonic settings in the Cenozoic. *Sedimentology in the 21st century – a tribute to Wolfgang Schlager. Sed. Geol.*, **175**, 49–72.
- Boylan, A.L., Waltham, D.A., Bosence, D.W.J., Badenas, B and Aurell, M. 2002. Digital rocks: linking forward modelling to carbonate facies. *Basin Res.*, **14**, 401–415.

- Brack, P., Rieber, H. and Urlichs, M., 1999. Pelagic successions in the Southern Alps and their correlation with the Germanic Middle Triassic. *Zbl. Geol. Paläontol., Teil I*, **7-8**, 853-876.
- Broecker, W.A. and Takahashi, T. 1966. Calcium carbonate precipitation on the Bahama Banks. *J. Geophys. Res.*, **71**, 1575–1602.
- Bredehoeft, J.D. and Konikow, L.F. 2012. Groundwater models: validate or invalidate. *Groundwater*, **50**, 493-495.
- Burgess, P.M. 2013. CarboCAT: A cellular automata model of heterogeneous carbonate strata. *Comput. Geosci.*, **53**, 129-140.
- Burgess, P.M., Lammers, H., Van Oosterhout, C. and Granjeon, D. 2006. Multivariate sequence stratigraphy: tackling complexity and uncertainty with stratigraphic forward modeling, multiple scenarios and conditional frequency maps. *AAPG Bull.*, **90**, 1883–1901.
- Casati, P. and Gnaccolini, M. 1967. Geologia delle Alpi Orobic occidentali. *Riv. It. Paleontol. Strat.*, **73**, 25-162.
- Cook, H.E., McDaniel, P.N., Mountjoy, E.W. and Pray, L.C. 1972. Allochthonous carbonate debris flows at Devonian bank ('reef') margins Alberta, Canada. *Bull. Can. Pet. Geol.* **20**, 439-497.
- Davies, G.R. 1977. Former magnesium calcite and aragonite submarine cements in Upper Paleozoic reefs of the Canadian Arctic: a summary. *Geology*, **5**, 11–15.
- Della Porta, G., Kenter, J.A., Bahamonde, J.R., Immenhauser, A., Villa, E. 2003. Microbial boundstone dominated carbonate slope (Upper Carboniferous, N Spain): microfacies, lithofacies distribution and stratal geometry. *Facies*, **49**, 175-207.
- Della Porta, G., Kenter, J.A., Bahamonde, J.R. 2004. Depositional facies and stratal geometry of an Upper Carboniferous prograding and aggrading high-relief carbonate platform (Cantabrian Mountains, N Spain). *Sedimentology*, **51**, 267-295.
- Demicco, R.W. and Hardie, L.A. 2002. The “carbonate factory” revisited: a reexamination of sediment production functions used to model deposition on carbonate platforms. *J. Sed. Res.*, **72**, 849–857.
- Dunham, R. 1962. Classification of carbonate rocks according to depositional texture. *AAPG Mem.*, **1**, 108–121.
- Eberli, G.P., Kendall, C.G.St.C, Moore, P., Whittle, G.L. and Cannon, R. 1994. Testing a seismic interpretation of great Bahama Bank with a computer simulation. *AAPG Bull.*, **98**, 981–1004.
- Enos, P. 1991. Sedimentary parameters for computer modeling. In: *Sedimentary Modeling: Computer Simulations and Methods for Improved Parameter Definition* (Eds E.K. Franseen. W.L. Watney. C.G.St.C. Kendall and W. Ross), *Kansas Geol. Surv. Bull.*, **233**, 63-99.
- Flory, R., Whitaker, F., Smart, P.L. and Reijmer, J.J.G. 2014. Submarine slope stability: Advances in modelling the anatomy of carbonate slope systems. *AAPG Congress, Houston, April 2014*.
- Fratantoni, D.M., 2001: North Atlantic surface circulation during the 1990's observed with satellite-tracked drifters. *J. Geophys. Res.*, **106**, 22067-22093.
- Frazer M.A., Whitaker F.F., Katz D., Harris P.M. and Hollis C. 2014. Understanding the development of an early, diagenetically-controlled template for reservoir quality distribution using forward sediment/diagenetic models of the Tengiz Platform, Kazakhstan. *AAPG Congress, Houston, April 2014*.
- Frisia-Bruni S., Jadoul F. and Weissert H. 1989. Evinosponges in the Triassic Esino Limestone (Southern Alps): documentation of early lithification and late diagenetic overprint. *Sedimentology*, **36**, 685-699.
- Frost, E.L. and Kerans, C. 2009. Platform-margin trajectory as a control on syndepositional fracture Patterns, Canning Basin, Western Australia. *J. Sed. Res.*, **79**, 44–55.
- Frost, E.L. and Kerans, C. 2010. Controls on syndepositional fracture patterns, Devonian reef complexes, Canning Basin, Western Australia. *J. Struct. Geol.*, **32**, 1231–1249.
- Gaetani M., Gnaccolini M., Jadoul, F. and Garzanti, E. 1998. Multiorder sequence stratigraphy in the Triassic system of the Western Southern Alps. In: *Mesozoic and Cenozoic sequence stratigraphy of European basins* (Eds P.C. de Graciansky, J. Hardenbol, T. Jacquin and P.R. Vail), *SEPM Spec. Publ.*, **60**, 701-717.
- Garcia-Fresca B., Sharp J.M. Jr, Lucia F.J., and Kerans C. 2012. Outcrop-constrained hydrogeological simulations of brine reflux and implications for early dolomitization of the Permian San Andres Formation. *AAPG Bulletin*, **96**, 1757-1781.
- Goldhammer, R.K., Dunn, P.A. and Hardie, L.A. 1990. Depositional cycles, composite sea-level changes, cycle stacking patterns, and the hierarchy of stratigraphic forcing: examples from Alpine Triassic platform carbonates. *Geol. Soc. Am. Bull.*, **102**, 535–562.
- Goldhammer, R.K. 1997. Compaction and decompaction algorithms for sedimentary carbonates. *J. Sed.Res.*, **67**, 26-35.
- Golomb, S.W. 1968. Mathematical models - Uses and limitations. *Astronaut. Aeronaut.*, **6**, 57-59.
- Grammer, G.M. and Ginsburg, R.N. 1992. Highstand versus lowstand deposition on carbonate platform margins: insight from Quaternary foreslopes in the Bahamas. *Mar. Geol.*, **103**,125-136.

- Grammer, G.M., Crescini, C.M., McNeill, D.F. and Taylor, L.H. 1999. Quantifying rates of syndepositional marine cementation in deeper platform environments – new insight into a fundamental process. *J. Sed. Res.*, **69**, 202-207.
- Hallock, P. 2001. Coral reefs, carbonate sediments, nutrients, and global change. In: *The History and Sedimentology of Ancient Reef Systems* (Ed. G.D.Stanley), 387–427.
- Harris, M.T. 1994. The foreslope and toe-of-slope facies of the middle Triassic Latemar buildup (Dolomites, Northern Italy). *J. Sed. Res.*, **B64**, 132-145.
- Hopley, D., Smithers, S. and Parnell, K. 2007. *The Geomorphology of the Great Barrier Reef*. Cambridge University Press, Cambridge.
- Hubbard, D.K., Miller, A.I. and Scaturro, D. 1990. Production and cycling of calcium carbonate in a shelf-edge reef system (St. Croix, U.S. Virgin Island): applications to the nature of reef systems in the fossil record. *J. Sed. Res.*, **60**, 335–360.
- Jadoul F., Gervasutti M. and Fantini Sestini N. 1992. The Middle Triassic of the Brembana Valley: Preliminary study of the Esino Platform evolution (Bergamasc Alps). *Riv. It. Paleontol. Strat.*, **98**, 299–324.
- Keim, L. and Schlager, W. 1999. Automicrite facies on steep slopes (Triassic, Dolomites, Italy). *Facies*, **41**, 15-25.
- Keim, L. and Schlager, W. 2001. Quantitative compositional analysis of a Triassic carbonate platform (Southern Alps, Italy). *Sed. Geol.*, **139**, 261-283.
- Kenter, J.A.M. 1990. Carbonate platform flanks: slope angle and sediment fabric. *Sedimentology*, **37**, 777-794.
- Kenter, J.A.M., Harris, P. M. M., Della Porta, G. 2005. Steep microbial boundstone-dominated platform margins—examples and implications. *Sed. Geol.*, **178**, 5-30.
- Konikow, L.F., and Bredehoeft, J.D. 1992. Ground-water models cannot be validated. *Adv. water resour.*, **15**, 75-83.
- Koša, E. and Hunt, D.W. 2005. Growth of syndepositional faults in carbonate strata: Upper Permian Capitan platform, New Mexico, USA. *J. Struct. Geol.*, **27**, 1069-1094.
- Kutzbach, J.E. and Gallimore, R.G. 1989. Pangean climates: Megamonsoons of the megacontinent. *J Geophys Res*, **94**, 3341-3357.
- Lucia, F.J. 2007. *Carbonate reservoir characterization*. Springer-Verlag Berlin Heidelberg, 341 pp.
- Marangon, A., Gattolin, G., Della Porta, G., Preto, N. 2011. The Latemar: A flat-topped, steep fronted platform dominated by microbialites and syndepositional cements. *Sed. Geol.*, **240**, 97-114.
- Markello, J.R., Koepnick, R.B., Waite, L.E. and Collins, J.F. 2008. The Carbonate Analogs Through Time (CATT) hypothesis and the global atlas of carbonate fields – a systematic and predictive look at the Phanerozoic carbonate systems. In: *Controls on Carbonate Platform and Reef Development* (Eds J. Lukasik and T. Simo), *SEPM Spec. Publ.*, **89**, 15–45.
- Maurer, F. 2000. Growth mode of Middle Triassic carbonate platforms in the Western Dolomites (Southern Alps, Italy). *Sed. Geol.*, **134**, 275-286.
- McNeill, D.F., Janson, X., Bergman, K.L. and Eberli, G.P. 2010. Belize: A Modern Example of a Mixed Carbonate–Siliciclastic Shelf. In: *Carbonate Depositional Systems: Assessing Dimensions and Controlling Parameters – The Bahamas, Belize and Persian/Arabian Gulf* (Eds H. Westphal, B. Riegl and G.P. Eberli), 81-143.
- Miller, C.R., James, N.P and Bone Y., 2012. Prolonged carbonate diagenesis under an evolving late Cenozoic climate; Nullabor Plain, southern Australia. *Sed. Geol.*, **261-262**, 33-49.
- Moses, C., Spate, A.P., Smith, D. I. and Greenaway, M. A. 1995. Limestone weathering in Eastern Australia. Part 2: Surface micromorphology study. *Earth Surf. Proc. Land.*, **20**, 501-514.
- Mundil, R., Zühlke, R., Bechstädt, T., Peterhänsel, A., Egenhoff, S. O., Oberli, F., Meier, M; Brack, P. and Rieber, H. 2003. Cyclicities in Triassic platform carbonates: synchronizing radio-isotopic and orbital clocks. *Terra Nova*, **15**, 81-87.
- Mutti, M. 1994. Association of tepees and paleokarsts in the Ladinian Calcare Rosso (Southern Alps, Italy). *Sedimentology*, **41**, 621-641.
- Paterson, R.J., Whitaker, F.F., Jones, G.D., Smart, P.L., Waltham, D. and Felce, G. 2006. Accommodation and sedimentary architecture of isolated icehouse carbonate platforms: insights from forward modelling with CARB3D+. *J. Sed. Res.*, **76**, 1162–1182.
- Paterson, R. J., Whitaker, F.F., Smart, P.L., Jones, G.D. and Oldham, D. 2008. Controls on early diagenetic overprinting in icehouse carbonates: insights from modelling hydrological zone residence times using CARB3D+. *J. Sed. Res.*, **78**, 251-281.
- Playton, TE., Janson, X and, Kerans, C. 2010. Carbonate slopes. In: *Facies Models 4, GEOText 6* (Eds N.P. James and R.W. Dalrymple): Geological Association of Canada, St John's, Newfoundland, 449–476.
- Pomar, L. and Hallock, P. 2008. Carbonate factories: A conundrum in sedimentary geology. *Earth-Sci. Rev.*, **87**, 134–169.
- Read, J.F. 1985. Carbonate platform facies models. *AAPG Bull.*, **69**, 1–21.

- Reijmer, J.J.G., Ten Kate, W.G.H.Z., Sprenger, A. and Schlager, W. 1991. Calciturbidite composition related to exposure and flooding of a carbonate platform (Triassic, Eastern Alps). *Sedimentology*, **38**, 1059-1074.
- Reijmer, J.J.G., Sprenger, A., Ten Kate, W.G.H.Z., Schlager, W. and Krystyn, L. 1994. Periodicities in the composition of Late Triassic calciturbidites (eastern Alps, Austria). *Orbital Forcing and Cyclic Sequences: IAS, Spec. Publ.*, **19**, 323-343.
- Riding, R. and Liang, L. 2005. Seawater chemistry control of marine limestone accumulation over the past 550 million years. *Rev. Esp. Micropaleontol.*, **37**, 1-11.
- Schlager, W. 1999. Scaling of sedimentation rates and drowning of reefs and carbonate platforms. *Geology*, **27**, 183-186.
- Schmid, D.U. 1996. Mikrobolithe und Mikroinkrustierer aus dem Oberjura. *Profil*, **9**, 101-251.
- Schulz, M. and Schäfer-Neth, C., 1997. Translating Milankovitch climate forcing into eustatic fluctuations via thermal deep water expansion: a conceptual link. *Terra Nova*, **9**, 228-321.
- Sellwood, B.W. and Valdes, P.J., 2006. Mesozoic climates: general circulation models and the rock record. *Sed. Geol.*, **190**, 269-287.
- Smith, S.V. and Kinsey, D.W. 1976. Calcium carbonate production, coral reef growth, and sea-level change. *Science*, **194**, 937-939.
- Stanley, S.M., Hardie, L.A. 1998. Secular oscillations in the carbonate mineralogy of reef-building and sediment-producing organisms driven by tectonically forced shifts in seawater chemistry. *Palaeogeogr. Palaeoclimatol. Palaeoecol.*, **144**, 3-19.
- Schwarzacher, W., Haas, J. 1986. Comparative statistical analysis of some Hungarian and Austrian Upper Triassic peritidal carbonate sequences. *Acta Geologica Hungarica*, **29**, 175-196.
- Warrlich, G.M.D., Waltham, D.A. and Bosence, D.W.J. 2002. Quantifying the sequence stratigraphy and drowning mechanisms of atolls using a new 3-D forward stratigraphic modelling program (CARBONATE 3D). *Basin Research*, **14**, 379-400.
- Warrlich, G.M.D., Bosence, D.W.J., Waltham, D.A., Wood, C., Boylan, A. and Badenas, B. 2008. 3-D stratigraphic forward modeling for analysis and prediction of carbonate platform stratigraphies in exploration and production. *Mar. Petrol. Geol.*, **25**, 35-58.
- Weber, L.J., Francis, B. P., Harris, P.M. and Clark, M. 2003. Stratigraphy, facies, and reservoir distribution, Tengiz Field, Kazakhstan. *AAPG Mem.*, **83**, 351-394.
- Whitaker, F.F. and Smart, P.L. 1997. Groundwater circulation and geochemistry of a karstified bank-marginal fracture system, South Andros Island, Bahamas. *J. Hydrol.*, **197**, 293-315.
- Whitaker, F. F. and Smart, P. L. 2007a. Geochemistry of meteoric diagenesis in carbonate islands of the northern Bahamas: 1. Evidence from field studies. *Hydrol. Process.*, **21**, 949-966.
- Whitaker, F. F. and Smart, P. L. 2007b. Geochemistry of meteoric diagenesis in carbonate islands of the northern Bahamas: 2. Geochemical modelling and budgeting of diagenesis. *Hydrol. Process.*, **21**, 967-982.
- Whitaker, F. F., Smart, P. L., Hague, Y., Waltham, D. A. and Bosence, D. J. 1997. A coupled two-dimensional sedimentological and diagenetic model for carbonate platform evolution. *Geology*, **25**, 175-178
- Whitaker, F.F., Smart, P.L., Hague, H., Waltham, D., and Bosence, D. 1999. Structure and function of a coupled two-dimensional diagenetic and sedimentological model of carbonate platform evolution. In: *Numerical Experiments in Stratigraphy* (Eds. J.H., Harbaugh, W.L., Watney, E.C., Rankey, R., Slingerland, R.H., Goldstein and E.K., Franseen), *SEPM: Spec. Publ.* **62**, 339-356.
- Whitaker, F.F., Smart, P.L., Vahrenkamp, V.C., Nicholson, H. and Wogelius R.A. 1994. Dolomitization by near-normal sea-water? Field evidence from the Bahamas. In: *Dolomites: A Volume in Honour of Dolomieu* (Eds. B.H. Purser, M.E. Tucker & D.H. Zenger), *IAS Spec. Publ.* **21**, 111-132.
- Whitaker, F.F., Felce, G.P., Benson, G., Amour F, Mutti M. and Smart, P.L. 2014. Simulating fluid flow through forward sediment model stratigraphies: insights into climatic control reservoir quality in isolated carbonate platforms. *Petroleum Geoscience*, **20**, 27-40
- Williams, H.D., Burgess, P.M., Wright, V.P., Della Porta, G. and Granjeon D. 2011. Investigating carbonate platform types; multiple controls and a continuum of geometries: *J. Sed. Res.*, **81**, 18-37.
- Xiao, Y., Jones, G., Whitaker, F.F., Al-Helal, A., Stafford, S., Gomez-Rivas, E. and Guidry, S. 2013. Fundamental approaches to dolomitization and carbonate diagenesis in different hydrogeological systems and the impact on reservoir quality distribution. *International Petroleum Technology Conference, Beijing, China, March 26-28, 2013. IPTC Contribution 16579*, 16pp.
- Zühlke, R., Bechstäd, T. and Mundil, R. 2003. Sub-Milankovitch and Milankovitch forcing on a model Mesozoic carbonate platform—the Latemar (Middle Triassic, Italy). *Terra Nova*, **15**, 69-80.

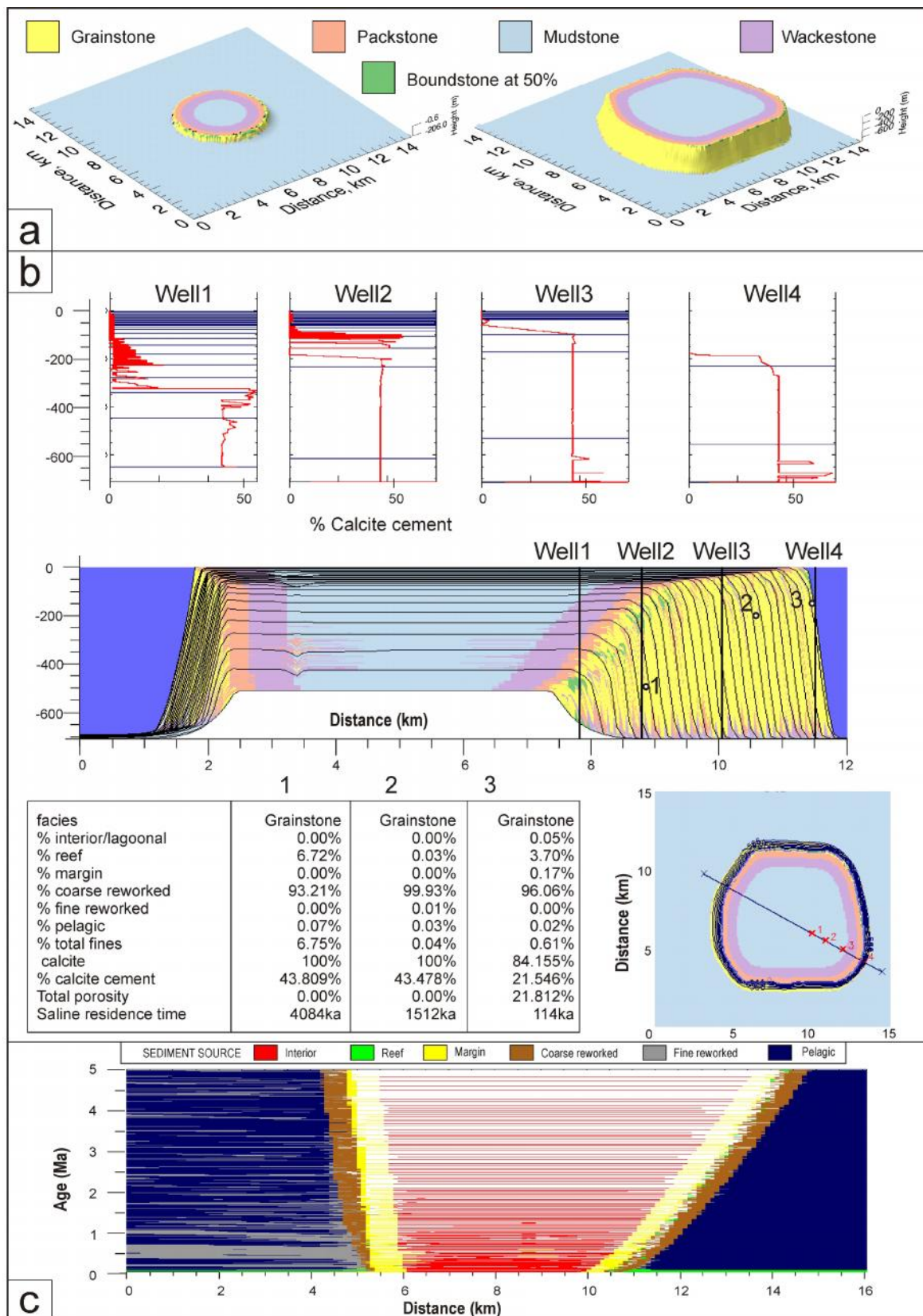


Fig. 1 – Examples of Carb3D+ output for the model discussed in the text: a) 3D view of the model at the initial stage (left) and at the end of the run (right); note the asymmetrical growth of the platform; b) cross section of the model with the position of user-selected wells showing the results (in this case percentage of calcite cement) along the wells and point interrogation of the model with some or the results from each point; in the map the trace of the section in the model and the position of the wells (facies legend in a); c) chronostratigraphic chart along a cross section from the leeward (left) to the windward side (right) of the platform.

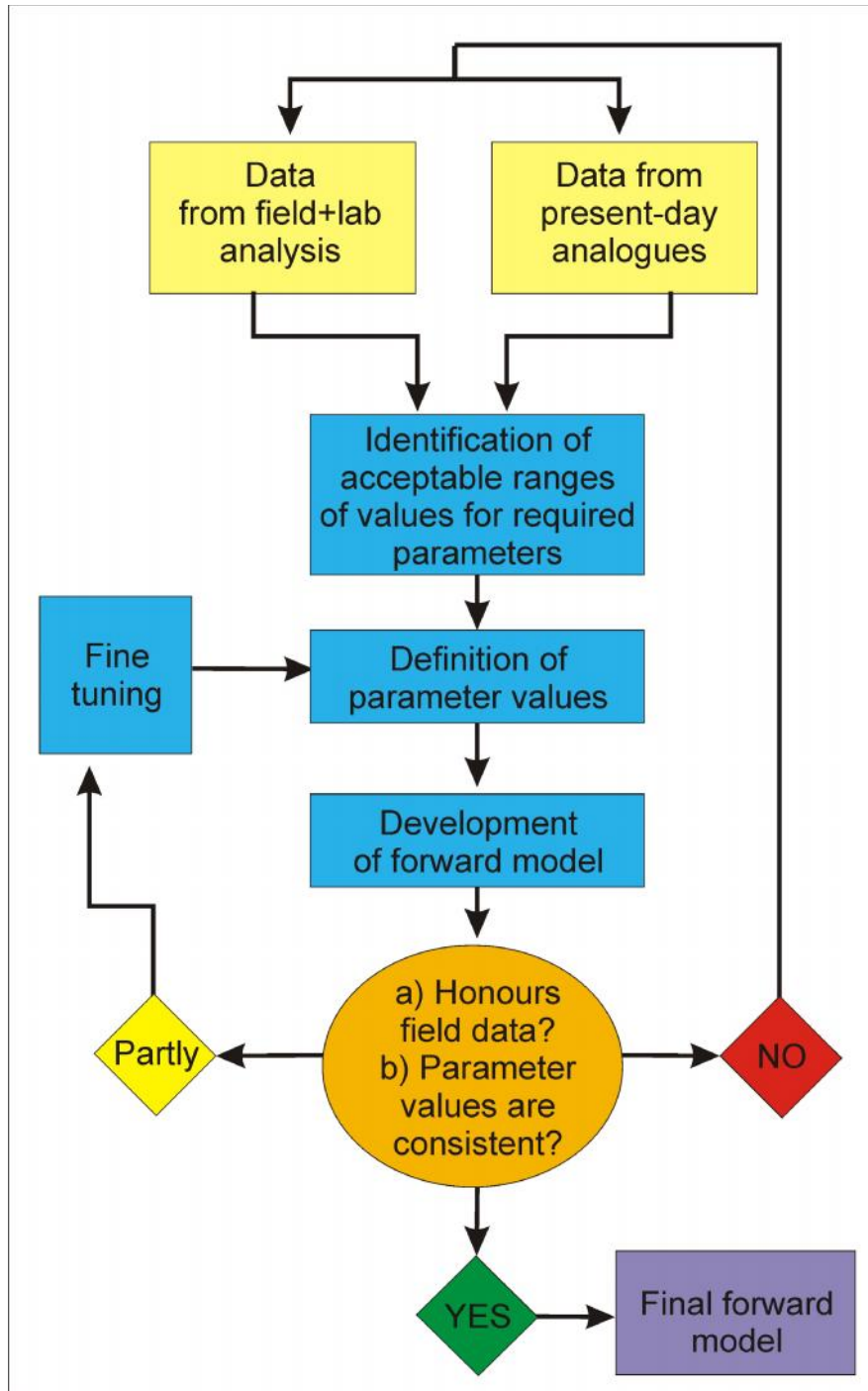


Fig. 2 – Workflow followed for the production of the final synthetic model of the studied platform with CARB3D+. Note the iterative process and the important role of field observation on the definition of the range of the required parameters and evaluation of developmental models.

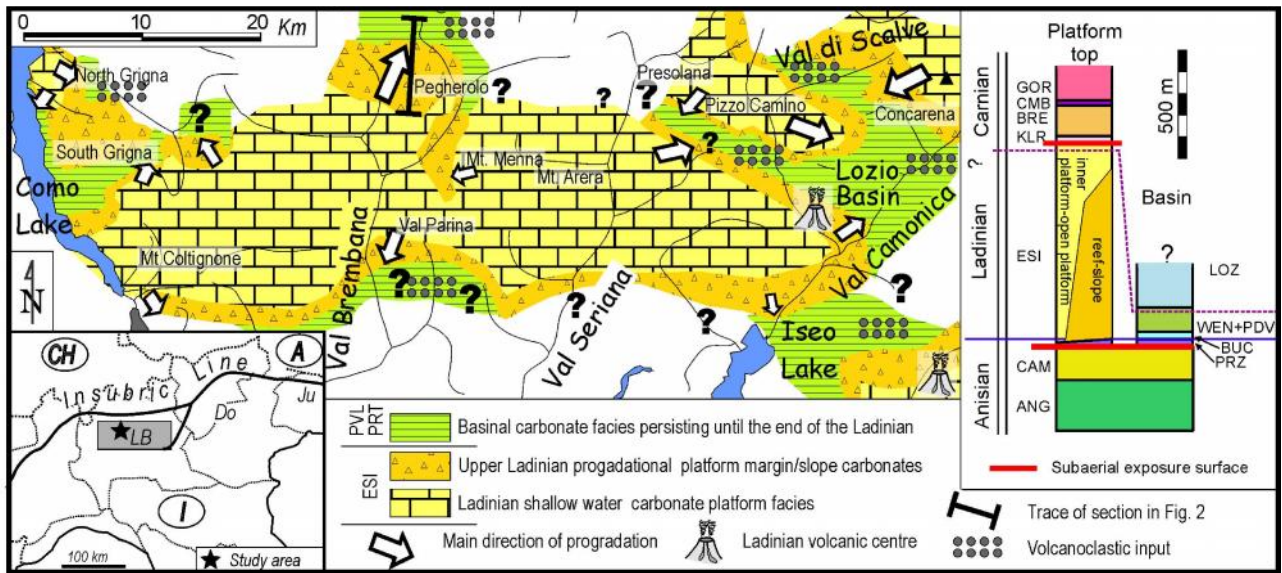


Fig. 3 – Ladinian paleogeography of the Central Southern Alps of Italy, with the position of the Pegherolo massif study area (dashed ellipse). Inset map the major domains of the Southern Alps (south of the Insubric line) are shown: Lombardy Basin (LB), Dolomites (Do) and Julian Alps (Ju). The simplified stratigraphic column show the relations between sequences on the platform top and basin, from Late Anisian to Early Carnian times. Lithostratigraphy: ANG: Angolo Limestone; CAM: Camorelli Limestone; PRZ: Prezzo Limestone; CUC: Buchenstein Fm., Wen: Wengen Formation; PDV: Perledo Varenna Limestone; LOZ: Lozio Shale; ESI: Esino Limestone; KLR: “Calcare Rosso”; BRE: Breno Fm.; CMB: “Calcare Metallifero Bergamasco”; GOR: Gorno Formation. I: Italy, CH: Switzerland, A: Austria. Modified after Berra et al. (2011).

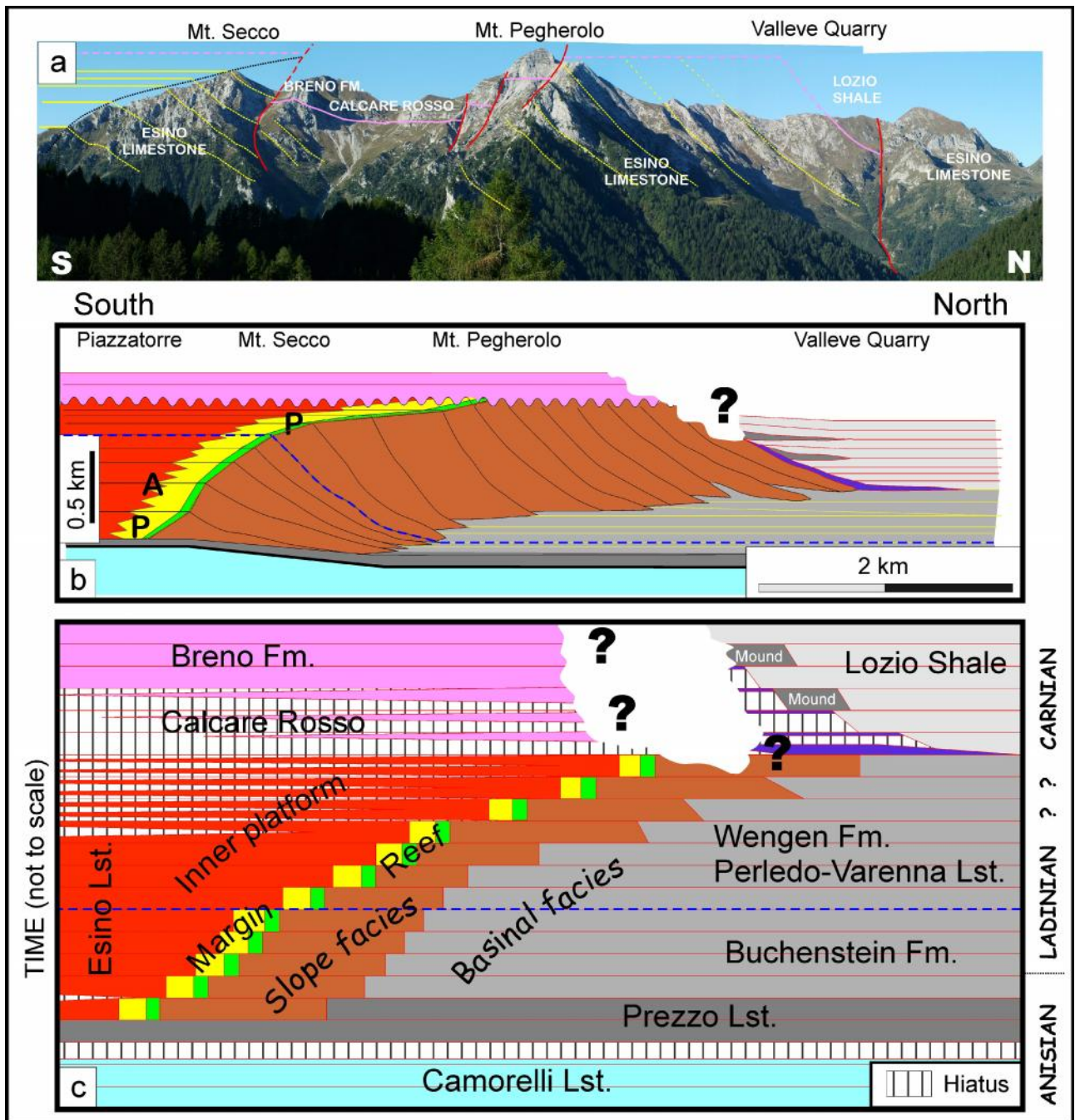


Fig. 4 – Above: Panoramic view of the Pegherolo massif from East, showing the northward progradation of the Esino Limestone. Field of view is about 4 km (red line: fault, pink line: top of the Esino Limestone; yellow line: bedding; black dashed line: possible reef trajectory). Centre: depositional architecture of the Pegherolo Massif interpreted from outcrop observations and analysis of samples (the blue dotted line marks the base of the rapidly prograding slope facies). Below: qualitative chronostratigraphic reconstruction of the stratigraphic sketch. Modified after Berra et al. (2011).

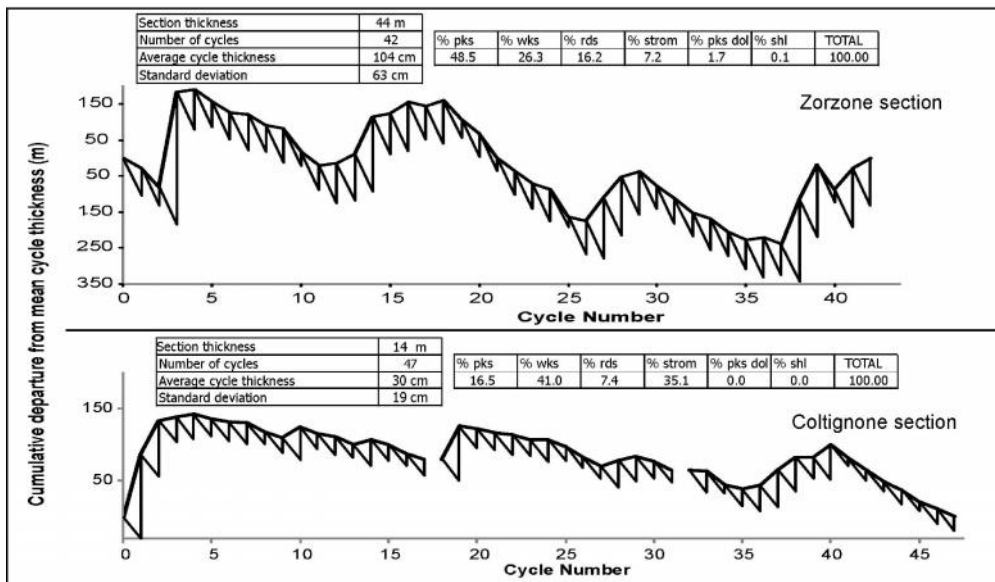
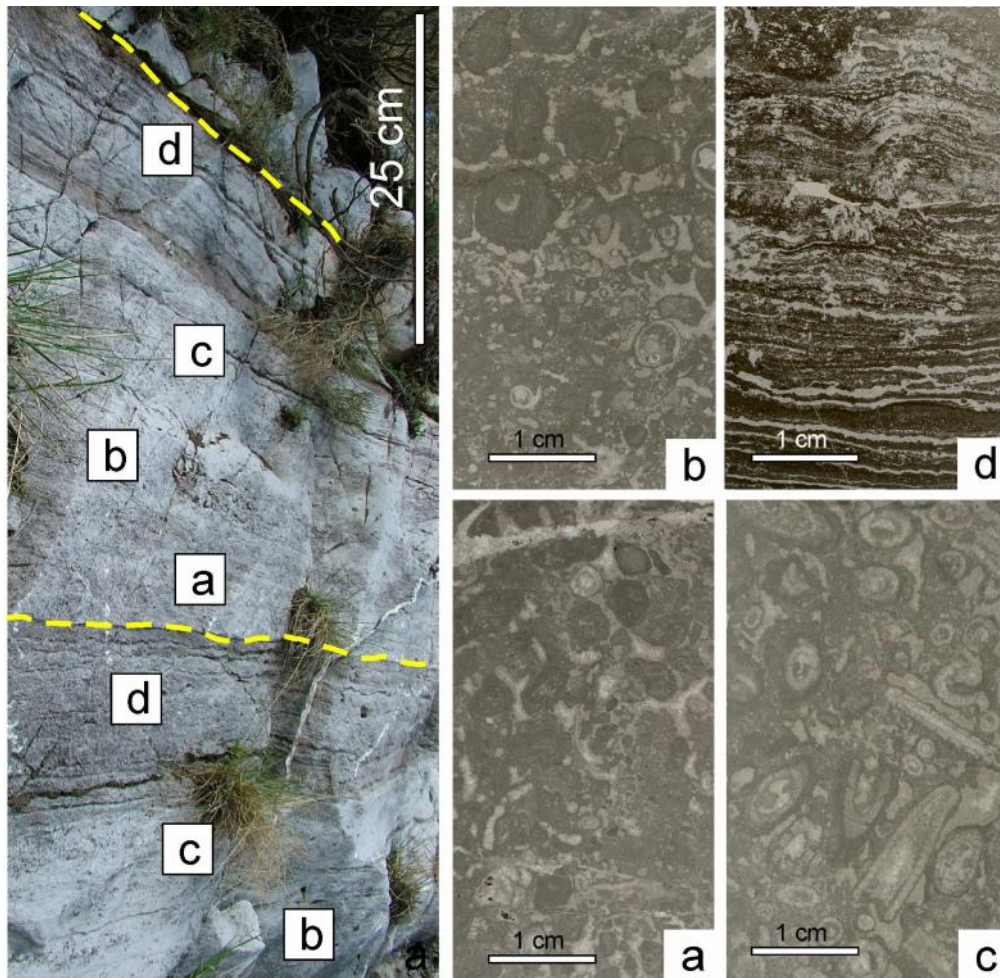


Fig. 5 – Above: cyclic organization and microfacies of the different facies identified in the platform interior domain of the Esino Limestone and facies details. On the right; cyclic organization in outcrop of the Esino Limestone, the yellow dashed lines mark the boundary of the cycles. Letters from (a) to (d) indicate the position in the cycles of the facies shown on the right in photographs of scanned thin sections (a: bio/intraclastic packstone; b: oncoidal packstone/grainstone; c: bioclastic (mainly dasycladacean algae) packstone/grainstone; d: stromatolitic boundstone). Below: Fischer plots of platform interior cycles in the aggrading (above) and in the prograding (lower) part of the platform based on logs from Zorzone and Coltignone sections respectively. Tables show data on cyclicity and relative abundance of the identified facies (pks: packstone; wks: wackestone; rds: rudstone; strom: stromatolitic boundstone; pks dol: dolomitized packstone; shl: shale).

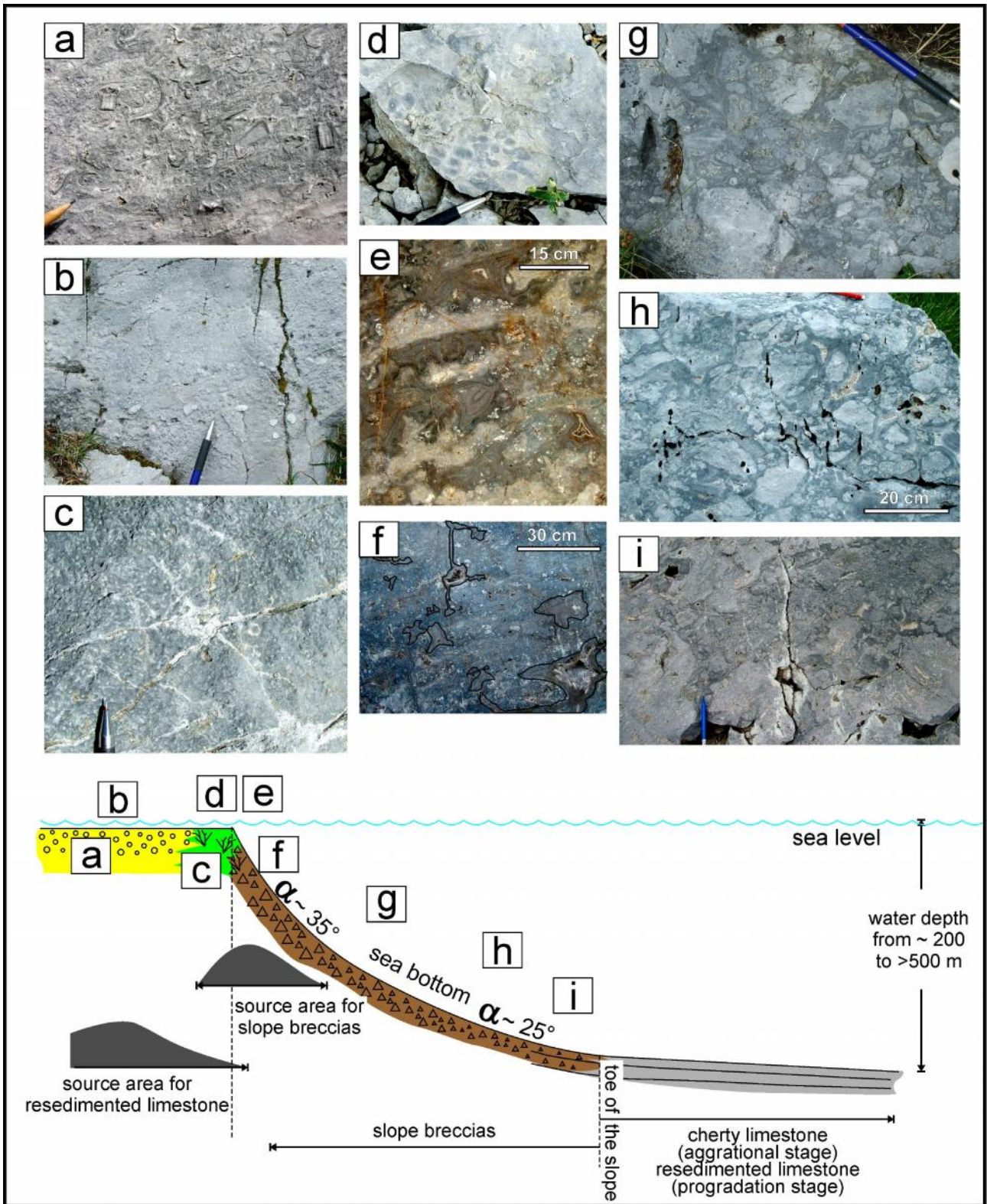


Fig. 6 - Facies distribution along an idealised depositional profile (below) from the back reef area to the basin (margin-reef-slope) of Esino Limestone, illustrated using outcrop photographs (a-i). a, b): bioclastic packstone, margin; c, d, e, f) reef and upper slope facies, respectively *Tubiphytes* boundstone (c), coral colony (d) and microbial mounds in the reef area (e, f); g, h, i): clast-supported, mud free, cemented slope breccias, with different degree of selection.

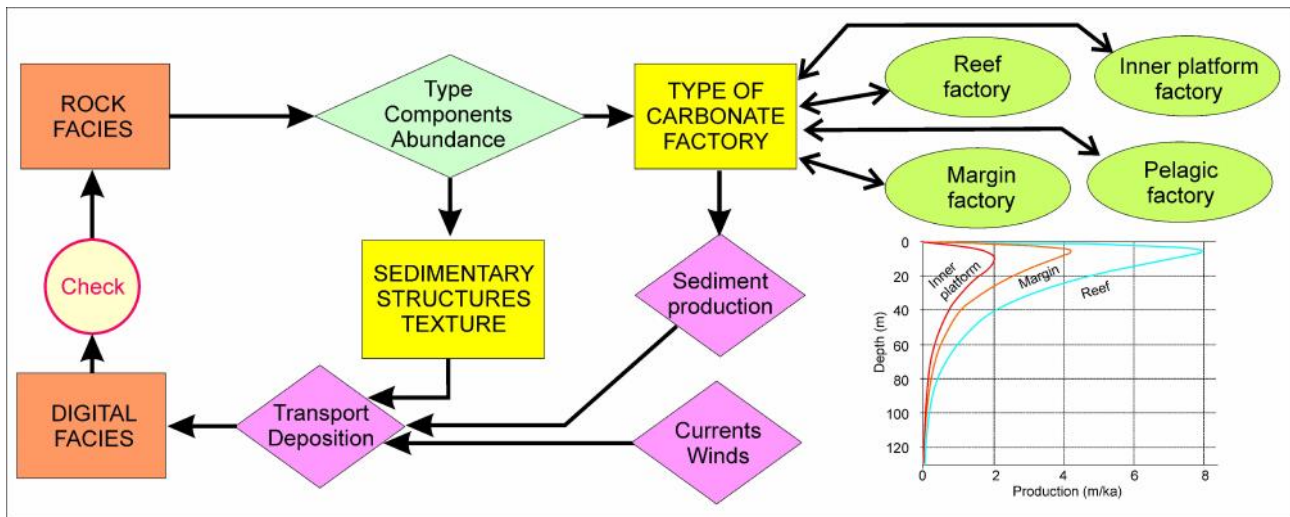


Fig. 7 – Schematic representation of the inputs and processes for modelling carbonate production and sediment transport/deposition. The field data, mainly including indications of the sediment composition (and thus source area), as well as sedimentary structures (indicative of transport processes) help in constraining the parameter values that control the digital facies produced by the model.

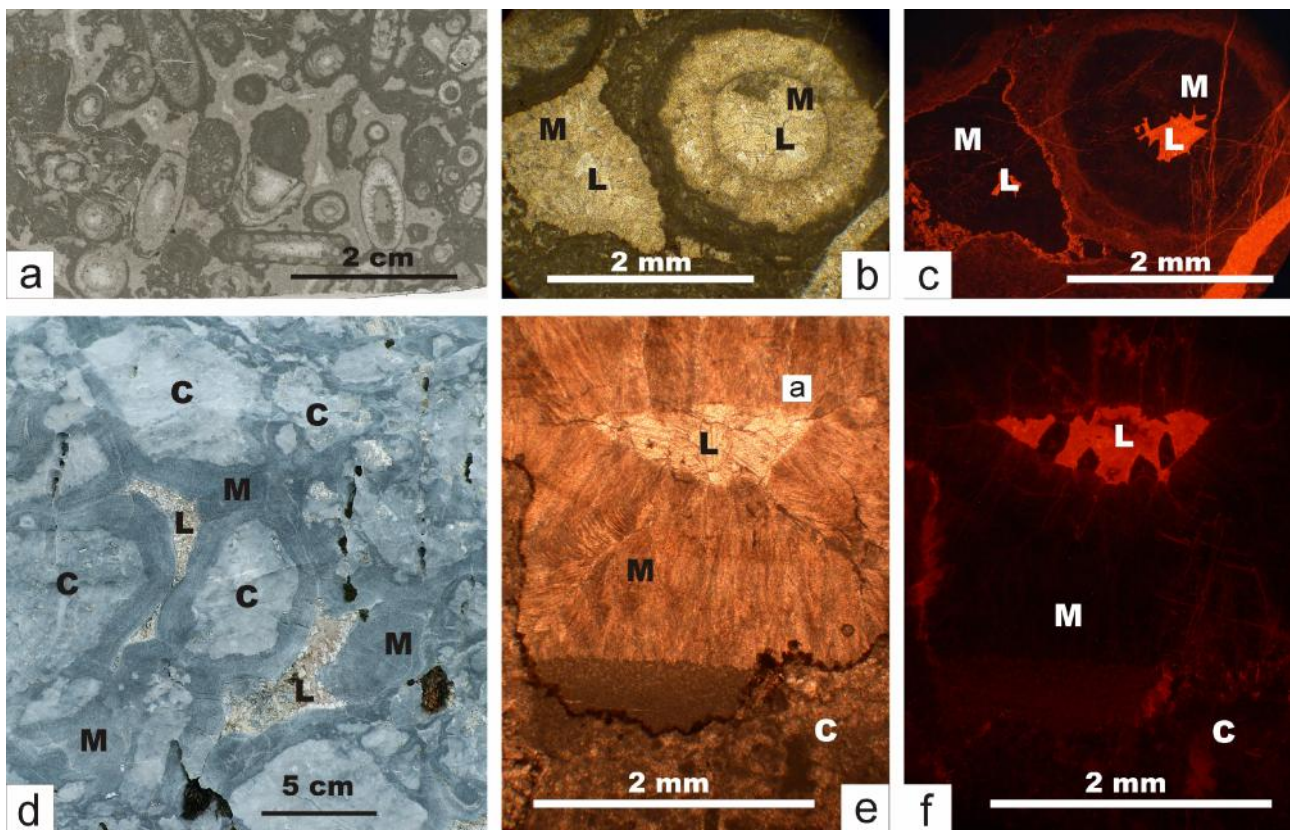


Fig. 8 – Constraints on the diagenetic history of the Esino Limestone. Both in the platform interior facies (a, b and c) and in the slope facies (d, e and f) it is possible to identify an early stage of cement precipitation (M) which consist of isopachous cloudy crystals completely black in cathodoluminescence (c and f), which commonly envelop the clasts (C) of the coarse slope breccias (d). The pore closure (both inter- and intra-particle, b and c) is mainly related to this event, whose origin is marine (Frisia-Bruni et al., 1989). The residual porosity after this event is documented by late (L) cements which are luminescent in cathodoluminescence, related to burial.

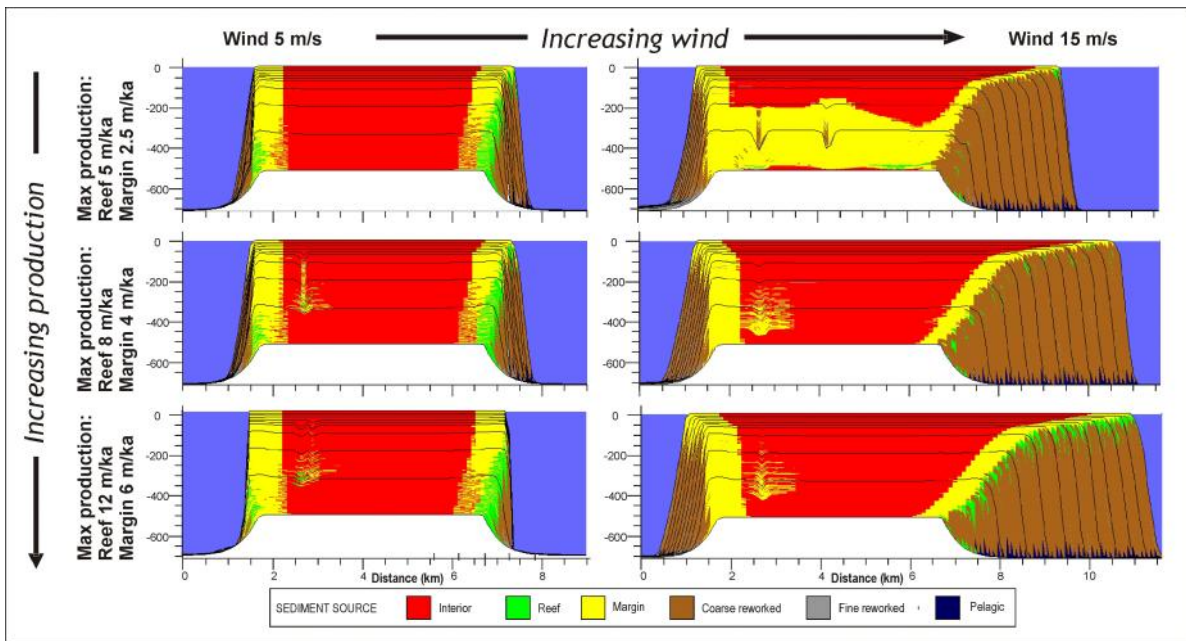


Fig. 9 – Example of results of a sensitivity analysis to evaluate the interactions between carbonate productivity and wind speed in controlling platform geometry and distribution of sediments. Black lines in this and following cross sections are timelines representing the sediment surface at intervals of 200 ka.

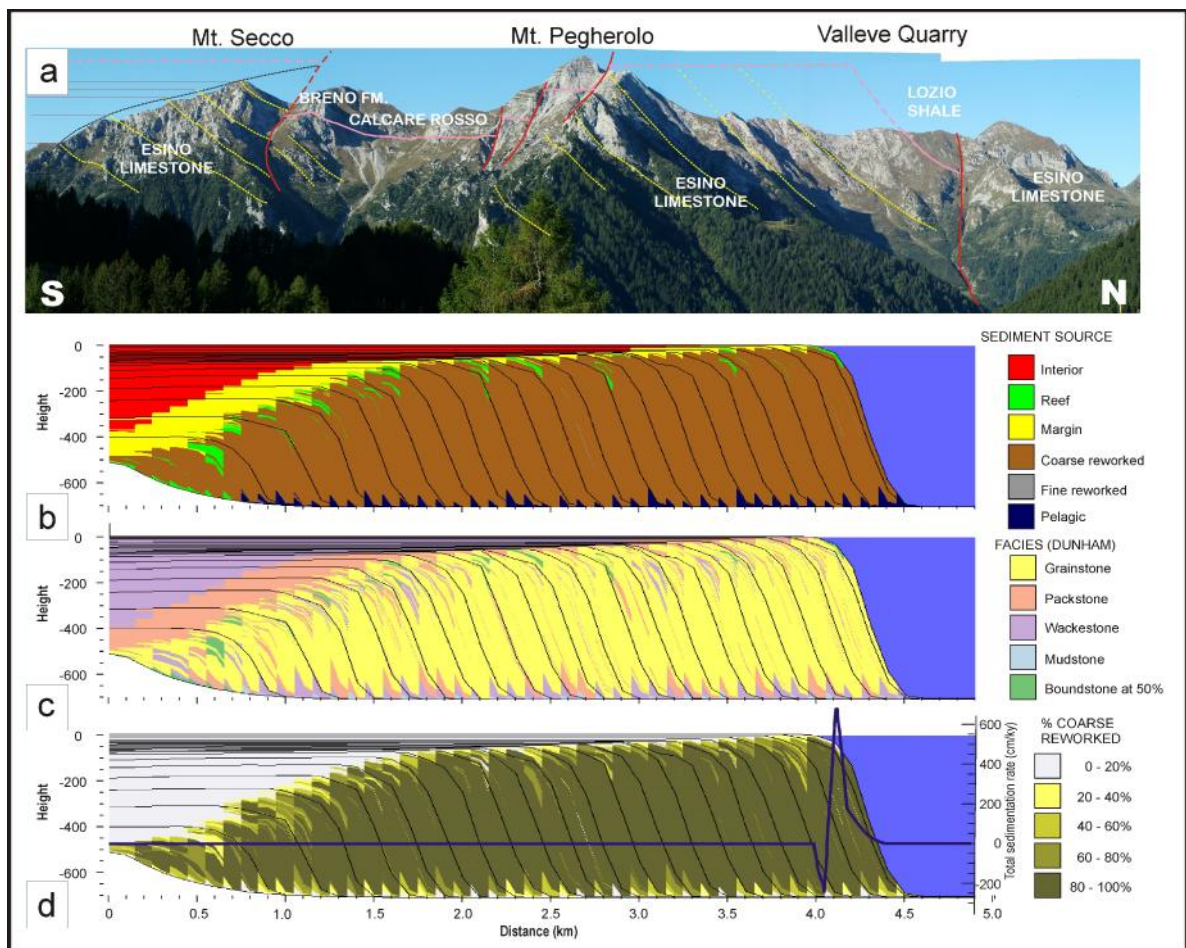


Fig. 10 – Comparison between geometry observed in the field (a) and a 2D section of the windward margin of the synthetic platform enabling evaluation of the source area for the sediments (b), sediment texture (c) and percentage of coarse reworked sediments (d). The blue line in (d) is the total sediment accumulation rate (scale on the right of the figure) showing most rapid accumulation in the upper slope with material sourced from erosion of the reef belt (negative accumulation rates). Production is zero on the platform top as this curve relates to the final depositional event during which the platform top was exposed.

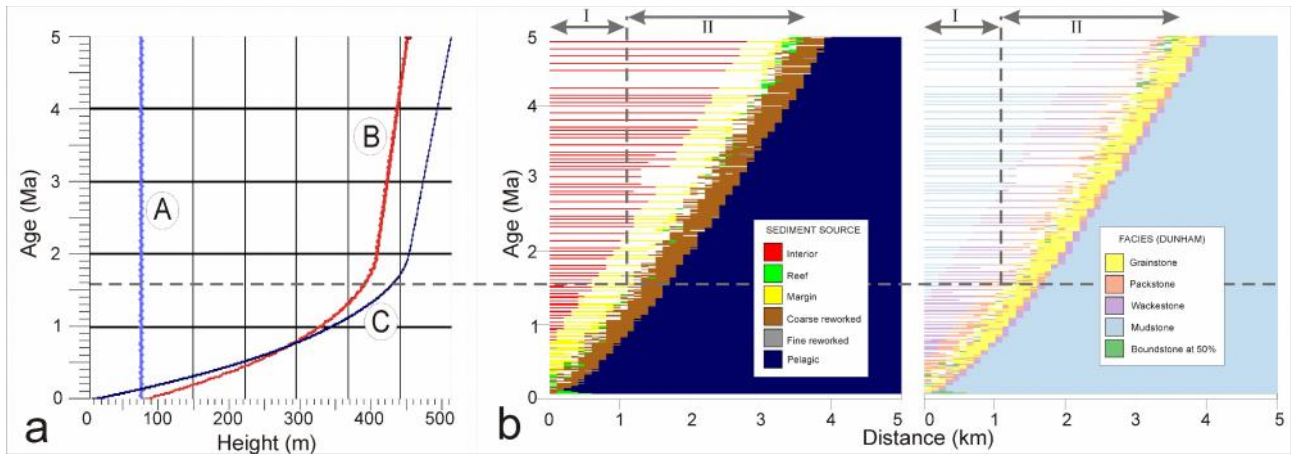


Fig. 11 Accommodation curve (a, left) and chronostratigraphic chart (b, right) for windward side of the synthetic platform produced by CARB3D+, with sediment source and facies. The decrease in creation of accommodation space (around 1.7 Ma) is indicated by the horizontal dashed line. Above this line, the hiatuses in the inner platform area increase, as a consequence of reduced accommodation: the arrows on the top of (b) indicate the time interval with highest (I) and lowest (II) aggradation/progradation ratio. The absolute progradation rate does not change through time, but the aggradation/progradation rate does, producing the geometry observed in fig. 10. The total accommodation curve (C) is the result of the general sea-level curve (B) and the high-frequency cycles and the assigned constant subsidence rate (A).

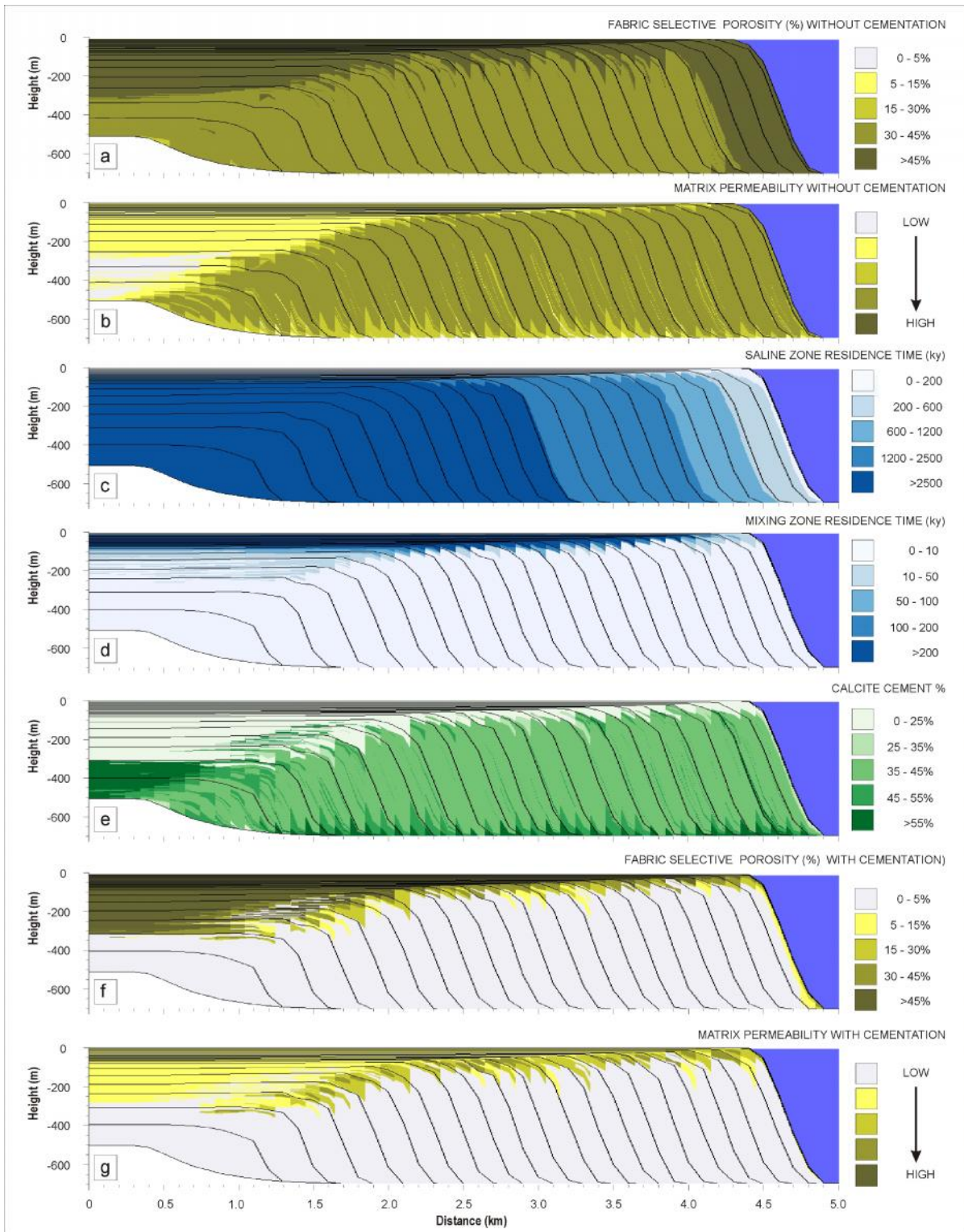


Fig. 12 – Modelling physical properties: without marine cementation (diagenesis off) the fabric selective porosity (a) is higher in the fine-grained facies of the inner platform and on the last prograding slope facies, but permeability (b) is strongly reduced in the fine-grained inner platform facies, where compaction further reduces permeability in the oldest fine-grained deposits. Switching diagenesis on, it is possible to evaluate the saline (c) and mixing (d) residence time: high saline residence time in most of the platform is responsible for the precipitation of early marine cements, whereas mixing residence time is significant during the last stages of the platform evolution, when accommodation was reduced, exposure periods were longer and significant diagenetic overprinting occurred, Cementation (e), dominating in the slope facies, heavily affect porosity (f), filling pores of the coarse-grained slope facies (compare with (a), where cementation is not simulated). The combined effects of compaction and cement precipitation produce a permeability distribution (g) controlled by the interplay between cementation (mainly in the slope facies) and compaction of the fine-grained sediments (mainly in the platform interior).

Types of parameters						
	Time	Initial surface	Accommodation	Sediment production	Oceanography	Diagenesis
Required values:	Age Cyclicality	Geometry (profile, size, bathymetry)	Relative sea-level curve (eustacy + subsidence/uplift)	Factories (inner platform, shoal margin, reef, basin) Production curves Restriction distance/depth	Currents Winds	Rainfall and evapotranspiration, initial mineralogy, dissolution and cementation
Constraints from:	Biostratigraphy Radiometric dating Fischer plots	Field reconstruction Geological mapping Stratigraphic sections	Platform architecture Sedimentological analyses Microfacies analyses		Present-day analogues Paleoclimate model	Cement paragenesis Cathodoluminescence Geochemistry

Tab. 1 - Types of parameters required by CARB3D+ to simulate development of a carbonate platform and major sources of information to constrain the acceptable range of values for any specific platform.

Waves	Wind speed	15 m/sec	Currents	Boundary speed	0.2 m/sec	Surface lowering	15 mm/ky
	Wind direction	300°±30		Current direction	330°	Annual rainfall	1000 mm/yr
	Friction coefficient	0.5		Roughness scale	1 mm	Actual evapotranspiration	700 mm/yr
				Tidal amplitude	0.8 m	Potential evapotranspiration	800 mm/yr
					Saline cementation rate	0.2% TRF/ka	
Carbonate production		Reef	Margin	Interior			
	Max production rate	8 m/ka	4 m/ka	1 m/ka			
	Depth of max prod.	5 m	5 m	4 m			
	Fall-off depth	25 m	25 m	10 m			
	Initial porosity	50%					
	Bioerosion % coarse	95%					
	Margin production cut-off			10 m			
	Margin % coarse			95%			
Restriction distance	0.5 km	1.2 km					
Restriction depth	50 m	50 m					
				Mineralogy		Aragonite	Calcite
				Pelagic	70	30	
				Reef	50	50	
				Margin	50	50	
				Interior	70	30	
				Fine sediments max entrainment rate		4 m/ka	
				Coarse sediments max entrainment rate		20 m/ka	

Tab. 2 - Key input parameters used for the model discussed in the text.